Virginia Water Resources Research Center
Virginia Polytechnic Institute and State University

Bulletin 163

A Study of Infiltration Trenches

C.Y. Kuo, J.L.Zhu, and L.A. Dollard

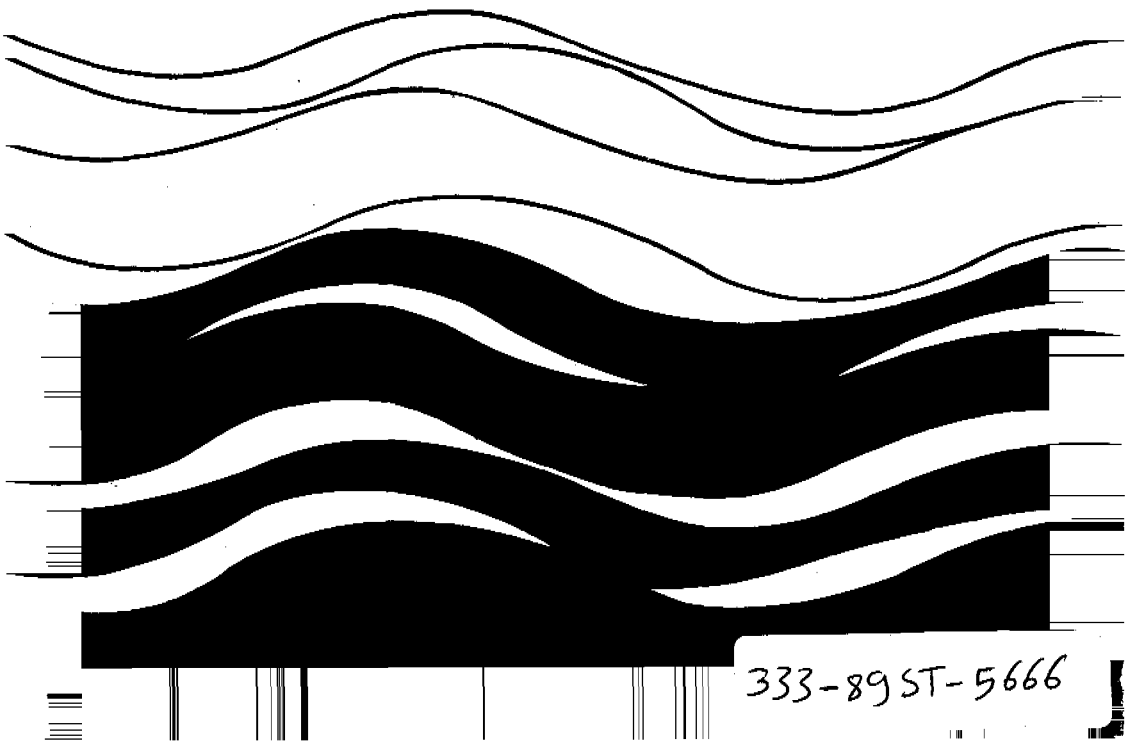

Bulletin 163
April 1989

A Study of Infiltration Trenches

C.Y. Kuo
J.L. Zhu
L.A. Dollard
Department of Civil Engineering
Virginia Polytechnic Institute and State University

VPI-VWRRC-BULL 163
3.5C

Virginia Water Resources Research Center
Virginia Polytechnic Institute and State University
Blacksburg • 1989

This Bulletin is published with funds provided in part by the
U.S. Geological Survey, Department of the Interior,
as authorized by the Water Resources Research Act of 1984.

Additional copies of this publication, while the supply lasts
may be obtained from the Virginia Water Resources Research Center.
Single copies are provided free to persons and organizations
within Virginia. For those out-of-state, the charge is $8 a copy.
Payment or purchase order must accompany all orders.

CONTENTS

LIST OF FIGURES

LIST OF TABLES

ACKNOWLEDGMENTS

The authors wish to express their appreciation to William Walker, Margaret Hrezo, and Diana Weigmann of the Water Center for administration of the project. Our thanks go, also, to the advisory committee and the technical reviewers of the manuscript. The work upon which this report is based was supported by funds provided by the Virginia Water Resources Research Center.

ABSTRACT

Urbanization increases peak flow and total volume of surface runoff as compared to predeveloped conditions. Infiltration trenches in unsaturated soil, one of the best management practices employed to control excessive runoff in urban areas, are examined in this report. A two-dimensional finite element model has been developed to simulate the transient flow in a variably saturated porous medium. Parameters such as soil properties, water table location, initial soil moisture condition, trench geometry, and surface runoff hydrograph at the facility site are specified, and routing is performed to find infiltration rate, water depth and storage in the trench, and overflow, if any. A laboratory model has also been used to test the validity of the finite element model and an infiltration model developed by Fok and his colleagues. Parametric studies have been performed with the finite element model for loam soil and sandy loam to determine the various effects of such parameters. Sands are recommended for use in an infiltration facility while clays are not. Saturated soil conductivity and the λ parameter from van Genuchten's model are found to have the greatest effect on infiltration rate. Where geometry is concerned, a wide, shallow trench is recommended for a given trench length and trench volume. A short, wide trench is recommended for a given depth and trench volume. The depth of the water table has been shown to have a greater effect in silt than in sand. There exists a limit for each soil beyond which the water table has no effect on infiltration. The limit is about 10 feet for sand, 30 feet for loamy sand, and 60 feet for sandy loam.

In the design of an infiltration trench, geometries vary considerably and water depth in the trench varies with time. The water flux across the bottom and sides of the trench is an important factor in sizing the trench. The finite element model has the capability to change geometries and to calculate the flux and water level in the trench. It is a useful tool in the design of infiltration facilities.

Key Words: Peak Flow, Runoff, Infiltration, Water Table, Trench Geometry

LIST OF SYMBOLS

a = well radius for Guelph Permeameter, L

A = gross cross-sectional area through which flow occurs, L^2

C_1, C_2 = C factors for Guelph Permeameter

C_u = coefficient of uniformity

D = soil/water diffusivity, L^2/T

D_{50} = median soil particle size, L

E = generalized specific water capacity, L^{-1}

f = volumetric flow rate via sources (or sinks) per unit volume of porous medium, L/T

h = pressure head, L

h_c = constant capillary potential head at wetting front, L

h_o = constant depth of water on soil surface, L

h_T = constant head loss in the transmission zone extrapolated to the wetting front, L

h_w = constant head loss in wetting front, L

h_x = horizontal pressure head loss, L

H = piezometric head, L

H_1, H_2 = well height for first and second measurements of Guelph Permeameter, L

K = hydraulic conductivity, L/T

K_{ij} = soil hydraulic conductivity tensor, L/T

K_s = saturated conductivity, L/T

n = porosity

n_i = unit vector normal to the surface of the control volume

q_i = vector of fluid velocity relative to the grains, L/T

Q = flow rate, L^3/T

Q_x = horizontal flow rate, L^3/T

r = number of nodal points in an element

$R_1 R_2$ = steady state rate of fall for Guelph Permeameter, L/T

s = degree of saturation

s_e = effective saturation

S_s = specific storage coefficient

t = time of infiltration, T

V = gross volume of the element, L^3

V_v = volume of voids, L^3

V_w = volume of water, L^3

w = test function

x = lateral advance of wetting front, L

X = reservoir constant for combined reservoirs in Guelph Permeameter, L^2

y = length of wetting from soil surface to wetting front during infiltration, L

Y = reservoir constant for inner reservoir only for Guelph Permeameter, L^2

α = compressibility of the porous medium

β = compressibility of the fluid

Γ = total boundary of the element domain, L

λ = parameter reflecting various types of soils, L^{-1}

μ = parameter reflecting various types of soils

ν = parameter reflecting various types of soils

Ω^e = element domain

ϕ_i = linear interpolation functions

ρ = fluid density, M/L^3

σ_z = normal intergranular stress on a horizontal plane, M/LT^2

θ = volumetric water content

θ_r = residual water content

θ_s = saturated water content

INTRODUCTION

It has been recognized that urbanization is responsible for the increase in both peak flow and total volume of surface runoff because of the decrease in infiltration as compared to predeveloped conditions. In many localities, the primary goal of stormwater management plans is to maintain, as nearly as possible, the predevelopment runoff characteristics. To control excessive runoff due to the increases in the impervious area of a watershed, detention basins, infiltration facilities, porous pavements, swales, marshes, and open spaces are commonly employed. These control structures, known as urban best management practices, have been proven to be effective in runoff and nonpoint source pollution control.

Infiltration facilities in unsaturated soil are examined in this report. An infiltration structure is defined as a dry well, pond, or subsurface trench that is used to temporarily store runoff in a stone-filled reservoir. It is generally used on relatively small drainage areas such as residential lots, commercial areas, parking lots, and open space areas. Surface runoff flows into the trench and infiltrates the surrounding soil media slowly. Infiltration facilities offer two major advantages in urban stormwater management. In terms of surface runoff control, they attenuate and reduce the peak runoff, reduce or eliminate the runoff volume. In terms of subsurface water management, they increase the local soil moisture and water table due to infiltration, and feed water into natural streams after the storm to augment the low streamflow. The facilities have great capability to trap nonpoint source pollutants associated with the runoff. However, pollutants collected in the facility itself have the potential to contaminate the unsaturated and saturated subsurface zones due to long term percolation.

Infiltration structures have been employed in many parts of the country. Higgs (1978) has designed percolation trenches to handle surface runoff from parking lots in Northern Virginia. A dry well has been designed and constructed to serve as a rain and snowmelt water catchbasin for a flat building roof and parking area in Canada (Beukeboom 1982). Infiltration basins are used to hold urban storm runoff in Florida and California (Hantzsche and Franini 1980). McBride and Sternberg (1983) at the University of Maryland developed a standardized method for selecting the optimum site for an infiltration facility and a design procedure for determining the storage volume required to control a known volume of runoff. Bouwer's steady state equation (1978) was used in their formulation. Design specifications and procedures are available (Ericsson and Gustafson 1982; South Florida Water Management District 1983; Maryland Department of Natural Resources 1984; Virginia Water Control Board 1978; Northern Virginia Planning District Commission 1978, 1987; Schueler 1987). Most of the design manuals deal with rational approaches and empirical

formulas. The principle of the conservation of mass is used in the calculation of the volume required for the infiltration structure. The infiltration rate is assumed to be constant for a given type of soil. In fact, the infiltration rate is a function of the location of the water table, the initial moisture condition of the soil, the water depth in the facility, etc. There is a need to rigorously analyze the infiltrations facilities by developing a computer model so that design variables such as dimensions and shape, properties of the aggregates in the facility and the surrounding soil, water table, surface runoff, infiltration rate, storage volume, detention time, etc., can be studied in detail.

Research on infiltration facilities is limited. Most of the research on infiltration itself has been conducted in connection with irrigation. The American Society of Agricultural Engineers (1983) sponsored a conference on advances in infiltration in which many different methods for estimating infiltration were discussed. Aron (in Poertner 1974) conducted a field experiment on infiltration trenches. This experiment used a sprinkler system to simulate rainfall and the infiltration trenches were equipped with observation wells. This experiment was limited in that only one site could be studied. Laboratory models of infiltration trenches are rare. Fok, Chung, and Clark (1982) used a laboratory model to verify their infiltration equations. However, this was not a model specifically for infiltration trenches. A study of infiltration trenches conducted by Yim and Sternberg (1984) at the University of Maryland used a laboratory model. The model used concrete sand as the porous medium with 3/8-inch gravel as aggregates in the infiltration trench. The model was used to test the validity of a theoretical infiltration equation proposed by Bouwer (1978). The model was also used to evaluate the effects of sediment accumulation on infiltration through the trench and to establish a practical method of controlling sediment load. The experiment validated Bouwer's equation and recommended a natural granular filter to trap sediments instead of a plastic fabric filter commonly used.

A simple analytical model for infiltration basins was given by Li (1983). This model considers the vertical infiltration only, neglecting the horizontal advance of the wetting front. Two-dimensional infiltration equations for furrow irrigation expressed in explicit forms have been developed by Fok and his colleagues (Fok and Hansen 1966; Fok 1967; Fok, Chung, and Clark 1982). Vertical and horizontal advances of the wetting front are calculated based upon Darcy's law and the principle of continuity. The cumulative infiltration volume in the model is calculated by multiplying the porosity of soil, the net increment in the degree of saturation, and the wetted volume. The unsteady two-dimensional water flow equation for unsaturated soils was solved numerically with a finite difference method using an alternating-direction implicit method by Selim and Kirkham (1974). The water table was considered as a water source in their model. However, a capillary fringe zone above the water table was not considered in

either Fok's model or the finite difference model. There are other computer models available in dealing with flow in unsaturated zones (Yeh 1987; Kaluarachchi and Parker 1987; and Huyakorn et al. 1986). They are not specifically formulated for the study of infiltration facilities. In the design of an infiltration trench, fo example, trench geometries vary considerably and water depth in the trench varies with time. The water flux across the bottom and the sides of the trench is an important factor in connection with sizing the trench. The computer model must have the capability to solve this particular problem.

The primary objective of this study is to develop a two-dimensional finite element model to simulate the transient flow of water in a variably saturated porous medium in order to calculate pressure heads and moisture distributions in the soil medium surrounding the infiltration facility and fluxes across the boundaries of the facility and the water table. The Galerkin finite element method is used. The advantages of using the finite element method include better computational efficiency, the ability to accommodate irregular geometries of the facilities and soil domains, and to yield the derivative type by-products such as flux at boundary points of the facility, which is the infiltration rate into the soil medium. Based on the soil properties, initial soil moisture condition, facility geometry, and surface runoff hydrograph at the facility site, routing is performed to find infiltration rate, water depth and storage in the facility, and overflow if any. From this information, the size of the infiltration facility is chosen such that the desirable runoff detention and retention is attained. A laboratory model has also been designed and constructed to test the validity of the finite element formulation and the infiltration model developed by Fok and his colleagues. The verified computer model has been used to aid the design of infiltration trenches.

GOVERNING EQUATIONS

I. Derivation of Governing Equations

Consider a control volume V in an elastic porous medium having a uniform moisture content. The control volume will be allowed to deform, but the solid is considered incompressible. The following definitions are used:

V = gross volume of element

V_v = volume of voids

n = porosity = V_v/V

V_w = volume of water

s = degree of saturation = V_w/V_v

θ = volumetric water content = $V_w/V = ns$

Applying the law of mass conservation, the flux of fluid mass across the surface of the control volume plus the fluid mass increase or decrease due to sources or sinks within the control volume must be equal to the rate of fluid mass storage within the control volume. This can be written in the indicial form:

$$\iiint_{V(t)} \rho f dV - \iint_{A(t)} \rho\, n_i\, q_i dA = \frac{\partial}{\partial t} \iiint_{V(t)} ns\rho dV \tag{2.1}$$

where ρ is the fluid density, f is the volumetric flow rate via sources (or sinks) per unit volume of porous medium, A is the surface of the control volume, n_i is a unit vector normal to the surface of the control volume, q_i is the vector of fluid velocity relative to the grains, and $i = 1,2,3$ is the implied summation convention. By using the Green's theorem to integrate the second term of the left-hand side and the Leibnitz rule to integrate the right-hand side, Equation (2.1) becomes

$$\rho f V(t) - \frac{\partial(\rho q_i)}{\partial x_i} V(t) = \frac{\partial(ns\rho)}{\partial t} V(t) + ns\rho \frac{\partial V}{\partial t} \tag{2.2}$$

Since lateral constraints on an aquifer prohibit significant horizontal deformation, it is assumed the volume element will deform only vertically. Thus, the compressibility of the granular skeleton is defined as

$$\alpha = \frac{-\Delta V/V}{\Delta \sigma_z} \tag{2.3}$$

where σ_z is the normal intergranular stress on a horizontal plane. The use of the definition of n and Equation (2.3) yields

$$\frac{\partial V}{\partial t} = -\alpha V \frac{\partial \sigma_z}{\partial t} \tag{2.4}$$

assuming the solid volume remains constant, i.e., $\Delta V = \Delta V_v$, we can write

$$\frac{\partial n}{\partial t} = \frac{1}{V}\frac{\partial V_v}{\partial t} - \frac{V_v}{V^2}\frac{\partial V}{\partial t} = \left(1 - \frac{V_v}{V}\right)\frac{1}{V}\frac{\partial V}{\partial t} = -(1-n)\alpha\frac{\partial \sigma_z}{\partial t} \tag{2.5}$$

The compressibility of the fluid is defined as the change of fluid density $\Delta\rho$ with respect to pressure change ΔP and is expressed as

$$\beta = -\frac{\Delta\rho/\rho}{\Delta p} \tag{2.6}$$

Thus, it follows

$$\frac{\partial \rho}{\partial t} = \beta\rho\frac{\partial p}{\partial t} \tag{2.7}$$

Substituting Equations (2.4), (2.5), and (2.7) into Equation (2.2), one arrives at

$$n\rho\frac{\partial s}{\partial t} + n\rho s\beta\frac{\partial p}{\partial t} - s\rho\alpha\frac{\partial \sigma_z}{\partial t} = -\frac{\partial(\rho q_i)}{\partial x_i} + \rho f \tag{2.8}$$

which is a general equation applicable to both steady and unsteady flow in an elastic medium with a degree of saturation s. When the media is saturated ($s = 1$ and $\partial s/\partial t = 0$), any change in static pore pressure head must immediately produce a change in the intergranular stress throughout the medium (Eagleson 1970). That is $\Delta\sigma_z = -\Delta P = \rho g \Delta h$, where h is pressure head. Then, the governing equation for saturated flow is

$$\rho S_s\frac{\partial h}{\partial t} = -\frac{\partial(\rho q_i)}{\partial x_i} + \rho f \tag{2.9}$$

where $S_s = \alpha\rho g\,\theta/n + \beta\rho g\theta$ is the specific storage coefficient. When media is unsaturated, compressibility terms of Equation (2.8) are unimportant. The equation governing unsaturated flow is obtained by dropping the last

two terms on the left-hand side of Equation (2.8) as

$$\rho\frac{d\theta}{dh}\frac{\partial h}{\partial t} = -\frac{\partial(\rho q_i)}{\partial x_i} + \rho f \tag{2.10}$$

where $d\theta/dh$ is the water capacity.

The Darcy's law in the vector form is

$$q_i = K_{ij}\frac{\partial H}{\partial x_j} \tag{2.11}$$

where K_{ij} is the soil hydraulic conductivity tensor, $H = h + x_2$ is the piezometric head, and x_2 is the vertical coordinate representing elevation. Substituting Equation (2.11) into the right-hand side of Equation (2.8) and combining Equation (2.9) and Equation (2.10), the following expression is derived for isothermal, compressible, laminar flow in an elastic porous medium.

$$E\frac{\partial h}{\partial t} = \frac{\partial}{\partial x_i}(K_{ij}\frac{\partial h}{\partial x_j} + K_{i2}) + \rho g\beta(K_{2j}\frac{\partial h}{\partial x_j} + K_{22}) + f \qquad (2.12)$$

where E is the generalized specific water capacity, which is usually written as $E = \omega S_s + d\theta/dh$, with $\omega = 1$ for $h \geq 0$ (saturated) and $\omega = 0$ for $h < 0$ (unsaturated).

If the principal directions of the hydraulic conductivity tensor coincide with those of coordinates (i.e. $K_{ij} = 0$ when $j \neq j$) and assuming incompressible fluid ($\beta = 0$), the two dimensional governing equation in x - y coordinate system can be derived from Equation (2.12) as

$$E\frac{\partial h}{\partial t} = \frac{\partial}{\partial x}(K_x(h)\frac{\partial h}{\partial x}) + \frac{\partial}{\partial y}(K_y(h)\frac{\partial h}{\partial y} + K_y(h)) + f \qquad (2.13)$$

where x and y indicate horizontal and vertical directions. In general, E = E(s) and K = K(s) are functions of the saturation and the saturation is a function of the pressure head s = s(h). There are a number of models for the soil properties. For example, the nonlinear functions to describe water capacity and hydraulic conductivity can be taken to be nonhysteretic and defined by van Genuchten (1980 a) as

$$\frac{d\theta}{dh} = \frac{\lambda\mu(\theta_s - \theta_r)}{1-\mu} S_e^{1/\mu}(1 - S_e^{1/\mu})^{\mu} \qquad (2.14)$$

$$K = K_s S_e^{1/2}[1 - (1 - s_e^{1/\mu})^{\mu}]^2 \qquad (2.15)$$

with

$$S_e = [1 + (\lambda|h|)^{\nu}]^{-\mu} \qquad (2.16)$$

where s_e is the effective saturation, θ_s is the saturated water content, θ_r is the residual water content, K_s is the saturated conductivity, and λ, μ and $\nu = 1/(1\times\mu)$ are parameters reflecting various types of soils.

II. Initial and Boundary Conditions

Initial conditions of pressure head must be specified at every nodal point in the domain

$$h(x,y,t) = h(x,y,0) \tag{2.17}$$

Either head or flux-type boundary conditions must be prescribed at the boundaries of the domain

$$h(x,y,t) = h(x_B, y_B, t) \tag{2.18}$$

or

$$-n_x K_x \frac{\partial h}{\partial x} - n_y (K_y \frac{\partial h}{\partial y} + K_y) = q(x_B, y_B, t) \tag{2.19}$$

where $h(x_B,y_B,t)$ and $q(x_B, y_B,t)$ are the prescribed pressure head and net fluid flux at the boundary and n_x and n_y are the components of unit normal vector on the boundary. Notice that $h(x_B,y_B,t)$ and $q(x_B,y_B,t)$ could be the known functions of time or could be determined from the model with which they are coupled. For example, given the initial water level in the trench and an input surface runoff hydrograph at the site, the water levels in the trench are always updated according to the changing of storage in the trench with time. In other words, the infiltration rate (i.e. the flux across the boundary of the trench) is a function of water depth in the trench. The water depth in the trench, which is related to the storage in the trench, influences the infiltration rate. All of these variables change with time. The dependency of storage on boundary condition is solved by a trial and error procedure. When the total flux is specified, the outflow flux will be computed based on a trial $h(x_B,y_B,t)$, then the computed flux is checked against the specified flux. Then $h(s_B,y_B,t)$ is adjusted until the difference between the specified flux and the computed flux is negligible.

I. Formulation

Multiplying Equation (2.13) with a test function w and integrating over an element domain Ω^e, one has

$$0 = \int_{\Omega^e} w\left\{E\frac{\partial h}{\partial t} - \frac{\partial}{\partial x}(K_x\frac{\partial h}{\partial x}) - \frac{\partial}{\partial y}(K_y\frac{\partial h}{\partial y} + K_y) - f\right\}dx\,dy \tag{3.1}$$

which can be further written in the variational form as

$$\begin{aligned} 0 = \int_{\Omega^e}\left\{wE\frac{\partial h}{\partial t} + \frac{\partial w}{\partial x}K_x\frac{\partial h}{\partial x} + \frac{\partial w}{\partial y}K_y\frac{\partial h}{\partial y} + K_y\frac{\partial w}{\partial y} - wf\right\}dx\,dy \\ - \int_{\Gamma^e} w\left\{K_x\frac{\partial h}{\partial x}n_x + (K_y\frac{\partial h}{\partial y} + K_y)n_y\right\}ds \end{aligned} \tag{3.2}$$

where Γ^e is the total boundary of the element domain Ω^e.
h can be approximated by the following expression

$$h(x,y,t) = \sum_{j=1}^{r} h_j(t)\phi_j(x,y) \tag{3.3}$$

where h_i are values of h at time t and at point (x_i,y_i), ϕ_i are linear interpolation functions, and r is the number of the nodal points in an element.

Substituting Equation (3.3) and $w = \phi_i$ into Equation (3.1), one obtains

$$\begin{aligned} 0 = \sum_{j=1}^{r}\Bigg[\left\{\int_{\Omega^e} E\phi_i\phi_j dx\,dy\right\}\frac{\partial h_j}{\partial t} \\ + \left\{(K_x\frac{\partial\phi_i}{\partial x}\frac{\partial\phi_j}{\partial x} + K_y\frac{\partial\phi_i}{\partial y}\frac{\partial\phi_j}{\partial y})dx\,dy\right\}h_j\Bigg] \\ - \int_{\Gamma^e}\phi_i q_n ds + \int_{\Omega^e} K_y\frac{\partial\phi_i}{\partial y}dx\,dy - \int_{\Omega^e} f\phi_i\,dx\,dy \end{aligned} \tag{3.4}$$

where

$$q_n = -n_x K_x\frac{\partial h}{\partial x} - n_y(K_y\frac{\partial h}{\partial y} + K_y) \tag{3.5}$$

which is defined as flux across boundary Γ^e. The finite element formulation of Equation (3.4) can also be written in the matrix form:

$$[M^e]\{\dot{h}\} + [K^e]\{h\} = \{F^e\} \tag{3.6}$$

where

$$M_{ij}^e = \int_{\Omega^e} E\phi_i\phi_j dx\, dy \tag{3.7}$$

$$K_{ij}^e = \int_{\Omega^e} \left\{ K_x \frac{\partial \phi_i}{\partial x} \frac{\partial \phi_j}{\partial x} + K_y \frac{\partial \phi_i}{\partial y} \frac{\partial \phi_j}{\partial y} \right\} dx\, dy \tag{3.8}$$

$$F_i^e = \int_{\Gamma^e} q_n \phi_i ds - \int_{\Omega^e} K_y \frac{\partial \phi_i}{\partial y} dx dy + \int_{\Omega^e} f \phi_i\, dx\, dy \tag{3.9}$$

If quadrilateral elements are used, i,j = 1,2,3,4, $[M^e]$ and $[K^e]$ are 4 x 4 matrices and $\{F^e\}$ is a vector of 4 components.

II. Isoparametric Elements and Numerical Integration

To facilitate an accurate representation of irregular domains, the isoparametric elements are used. However, it is difficult to compute the element coefficient matrices and column vectors directly in terms of the global coordinates x and y, which are used to describe the governing equation. This difficulty can be overcome by introducing an invertible transformation between a curvilinear element Ω^e and a master element $\hat{\Omega}$ of simple shape that facilitates numerical integration of the element equations. The coordinates in the master elements are chosen to be the natural coordinates (ξ,η) such that $-1 \leq (\xi,\eta) \leq 1$. Consider the coordinate transformation:

$$x = \sum_{i=1}^{4} x_i \hat{\phi}_i(\xi, \eta) \qquad y = \sum_{i=1}^{4} y_i \hat{\phi}_i(\xi, \eta) \qquad h = \sum_{i=1}^{4} h_i \hat{\phi}_i(\xi, \eta) \tag{3.10}$$

where the element interpolation functions are in natural coordinates, h_i is the solution at i th node of an element, and (x_i,y_i) are the global coordinates of the i th node of element Ω^e

$$\hat{\phi}_1 = \frac{1}{4}(1-\xi)(1-\eta) \qquad \hat{\phi}_2 = \frac{1}{4}(1+\xi)(1-\eta)$$

$$\hat{\phi}_3 = \frac{1}{4}(1+\xi)(1+\eta) \qquad \hat{\phi}_4 = \frac{1}{4}(1-\xi)(1+\eta) \tag{3.11}$$

In order to perform element calculations, one must transform functions of x and y to functions of ξ and η. The coordinate transformation of the integrals should be employed.

Let [J] be the Jacobian matrix

$$[J]=\begin{bmatrix} \dfrac{\partial x}{\partial \xi} & \dfrac{\partial y}{\partial \xi} \\ \dfrac{\partial x}{\partial \eta} & \dfrac{\partial y}{\partial \eta} \end{bmatrix} \tag{3.12}$$

and $[J]^{-1}$ be the inverse of the Jacobian matrix

$$[J]^{-1}=[J]^{*}=\begin{bmatrix} J_{11}^{*} & J_{12}^{*} \\ J_{21}^{*} & J_{22}^{*} \end{bmatrix} \tag{3.13}$$

In Equation (3.8) the integral is a function of x and y. Suppose that the mesh of finite elements is generated by a master element $\hat{\Omega}$. Using the transformation, the following equation is derived.

$$K_{ij}^{e}=\int_{\hat{\Omega}} \hat{K}_x\left(J_{11}^{*}\frac{\partial \hat{\phi}_i}{\partial \xi}+J_{12}^{*}\frac{\partial \hat{\phi}_i}{\partial \eta}\right)\left(J_{11}^{*}\frac{\partial \hat{\phi}_j}{\partial \xi}+J_{12}^{*}\frac{\partial \hat{\phi}_j}{\partial \eta}\right)+$$

$$\hat{K}_y\left(J_{21}^{*}\frac{\partial \hat{\phi}_i}{\partial \xi}+J_{22}^{*}\frac{\partial \hat{\phi}_i}{\partial \eta}\right)\left(J_{21}^{*}\frac{\partial \hat{\phi}_j}{\partial \xi}+J_{22}^{*}\frac{\partial \hat{\phi}_j}{\partial \eta}\right)J d\xi d\eta$$

$$=\int_{\hat{\Omega}} F(\xi,\eta)d\xi d\eta \tag{3.14}$$

Now the integral is defined over a rectangular master element and the quadrature can be presented in this form:

$$\int_{\hat{\Omega}} F(\xi,\eta)d\xi d\eta=\int_{-1}^{1}\left(\int_{-1}^{1} F(\xi,\eta)d\eta\right)d\xi=\sum_{I=1}^{M}\sum_{J=1}^{N} F(\xi_I,\eta_J)W_I W_J \tag{3.15}$$

where M and N denote the number of the quadrature points in the ξ and η directions, (ξ_I,η_J) denote the Gauss points, and W_I and W_J denote the corresponding Gauss weights. Mass matrix M_{ij} and force vector F_i are evaluated in the same way. Details involved in the numerical evaluation of element matrices has been shown by Reddy (1984).

III. Finite Difference Approximation in Time

Finite difference methods are typically used in the approximation of the time derivative. Equation (3.6) is approximated by a forward difference scheme as:

$$[\hat{K}^e]\{h^e\}^{k+1} = \{\hat{F}^e\} \tag{3.16}$$

where

$$[\hat{K}^e] = \omega[K^e]^{k+1} + \frac{1}{\Delta t}[M^e]^{k+1}$$

$$\{\hat{F}^e\} = (\frac{1}{\Delta t}[M^e]^{k+1} - (1-\omega)[K^e]^{k+1})\{h^e\}^k + \{F^e\}^{k+1} \tag{3.17}$$

IV. Solution Procedure

Based on the inter-element continuity conditions, all the element matrices are assembled into a global finite model, which is in general a system of equations in the form:

$$\begin{bmatrix} \hat{K}_{11} & \hat{K}_{12} & \hat{K}_{13} & \cdots & \hat{K}_{1n} \\ \hat{K}_{21} & \hat{K}_{22} & \hat{K}_{23} & \cdots & \hat{K}_{2n} \\ \hat{K}_{31} & \hat{K}_{23} & \hat{K}_{33} & \cdots & \hat{K}_{3n} \\ \vdots & \vdots & \vdots & \cdots & \vdots \\ \hat{K}_{n1} & \hat{K}_{n2} & \hat{K}_{n3} & \cdots & \hat{K}_{nn} \end{bmatrix} \times \begin{bmatrix} h_1^{k+1} \\ h_2^{k+1} \\ h_3^{k+1} \\ \vdots \\ h_n^{k+1} \end{bmatrix} = \begin{bmatrix} F_1 \\ F_2 \\ F_3 \\ \vdots \\ F_n \end{bmatrix} \tag{3.18}$$

This system of equations is solved by Gaussian elimination for values of h_j^{k+1} at time level k + 1. The nonlinearity (dependency of coefficient matrices on the solution) can be solved by an iterative method. The solution is attempted by a process of successive approximations. This involves making an initial guess and then improving the guess by some iterative process until an error criterion is satisfied.

An iterative scheme based on Newton-Raphson's method has been developed. Using indicial notation with the summation convention implied, Equation (3.18) can be written as

$$K_{ij}h_j - F_i = R_i \qquad i,j = 1,2,3, \ldots n. \tag{3.19}$$

where h_j is the approximation in current iteration and R_i is the residual. To minimize the residual, the improvement ΔH_j is found through

$$K_{ij}^{T} \Delta h_j = - R_i \tag{3.20}$$

where K^{T}_{ij} is the tangent or Jacobian matrix which is derived from Equation (3.19) as

$$K_{ij}^{T} = \frac{\partial R_i}{\partial h_j} = K_{i,k} \frac{\partial h_k}{\partial h_j} + \frac{\partial K_{ik}}{\partial h_j} h_k - \frac{\partial F_i}{\partial h_j} \tag{3.21}$$

V. Nodal Flux Computation

After convergence of the iterative solution has been achieved, the fluxes, q, along the head-type boundaries are determined by substituting the solution back into the global matrix equation for the rows that correspond to specified nonzero flux nodes.

$$\{q\} = [\hat{K}]\{h\}^{k+1} - \{\hat{F}\} \tag{3.22}$$

FINITE ELEMENT MODEL VERIFICATION

A computer code called "INFIL-FLOW" has been developed to simulate unsteady two-dimensional water flow in variably saturated porous media. The code is based on the Galerkin finite element formulation and the solution techniques that were described in previous chapters. To verify the code, three illustrative examples are presented. The examples are chosen from literature for the purpose of comparison.

I. 1-D Transient Vertical Flow

Geometry and boundary conditions of the problem are depicted in Figure 1. A flux of q = 3 cm/day is specified at the top boundary. The soil column has a depth of 150 cm with the water table located at the bottom where the boundary condition is the prescribed pressure head, h = 0. Fluxes, q = 0, are specified along the two vertical sides of the domain. The soil properties for loamy soil are described by van Genuchten's model (1980a) with this data: $\theta_r = 0.10$, $\theta_s = 0.45$, $\lambda = 0.025\ cm^{-1}$, $\nu = 1.65$, and $K_s = 50\ cm/day$. The initial pressure head distribution is taken to be the steady-state solution of 1-D Richards equation with zero flux at the top boundary and zero pressure head at the water table.

The results are compared in Figure 1 with that obtained by van Genuchten's 1-D finite element model (1980b). The deviations in moisture are about 1.5 percent near the top of the soil column. Agreements improve for the lower depths.

II. 2-D Transient Flow

Selim and Kirkham (1974) solved the 2-D diffusion-type flow equation for unsaturated soils using a finite difference method. With some modification to the "INFIL-FLOW," the same governing equation was solved by "INFIL-FLOW" using the same geometry and soil conditions. The governing equation in terms of soil moisture θ is

$$\frac{\partial \theta}{\partial t} = \frac{\partial}{\partial x}\left[D(\theta)\frac{\partial \theta}{\partial x}\right] + \frac{\partial}{\partial y}\left[D(\theta)\frac{\partial \theta}{\partial y}\right] + \frac{\partial K(\theta)}{\partial y} \qquad (4.1)$$

and soil water diffusivity, $D(\theta)$, and hydraulic conductivity, $K(\theta)$, are expressed as:

$$\begin{aligned} D(\theta) &= 3.33 \times 10^{-5} e^{29.34\theta}\ cm^2/\min \\ K(\theta) &= 3.33 \times 10^{-5} e^{54.11\theta}\ cm/\min \end{aligned} \qquad (4.2)$$

Initial water content is 0.20. The geometry and boundary conditions are shown in Figure 2 in which the results from both the Selim and Kirkham's model and the "INFIL-FLOW" are compared by lines of equal water content for time t = 10

min. and time = 50 min. For high water content contour lines, the comparison is excellent, but the fit is not very satisfactory near the wetting front where the low water content contour lines are located.

III. Steady-state Flow through a Square Embankment

Geometry and boundary conditions of the problem are depicted in Figure 3. No-flow boundary conditions exist at the base and top of the embankment. The water levels on the left- and right-hand side boundaries are 10 m and 2 m, respectively. On the seepage face, the pressure head is equal to zero. Along the boundary above the exit point, the flux normal to the boundary is zero. The height of exit point is an unknown and determined by trial and error procedures. Hydraulic properties are

$$s_e = \frac{A}{A + (|h - h_a|)^B} \qquad h < h_a \tag{4.3}$$

$$s_e = 1 \qquad h \geq h_a \tag{4.4}$$

$$K = K_s s_e^n \tag{4.5}$$

where A = 10 m, B = 1, and n = 1 are parameters, $h_a = 0$ is the air entry value (Huyakorn et al. 1986). Values of physical parameters used in the simulation are saturated conductivity $k_s = 0.01$ m/day, specific storage $S_s = 10^{-4}m^{-1}$,saturated and residual water contents $\theta_s = 0.25$ and $\theta_r = 0.2$. The results are compared to those obtained by Huyakorn et al. (1986) shown in Figure 3. The solutions for the location of water table and the distribution of base pressure head at the base are almost identical to those predicted by Huyakorn's model.

FOK'S TWO-DIMENSIONAL INFILTRATION MODEL

Fok et al. (1966, 1967, 1982) related infiltration rate to time. They found from experimental observations, that the relationship between length of wetting and time can be expressed as an exponential equation. They observed that when infiltration rates are plotted against corresponding infiltration times on a log-log paper, an exponential form is usually obtained. In this infiltration model, the soil is assumed to be homogeneous and unsaturated with a uniform initial moisture distribution. Also, the structure of the soil is assumed not to change after wetting. For two-dimensional flow, the loci of the wetting pattern are assumed to be half ellipses and the vertical and horizontal flow components are described by one-dimensional infiltration.

Fok et al. developed an equation for one-dimensional downward water movement in soil during infiltration. Darcy's Law

$$Q = KA\frac{h_T + y}{y} \tag{5.1}$$

was equated with the equation of continuity.

$$Q = nsA\frac{dy}{dt} \tag{5.2}$$

The resulting equation was integrated to arrive at an expression for downward soil water movement, and was rearranged such that

$$\frac{y}{h_T} - ln\,(1 + \frac{y}{h_T}) = \frac{tK}{nsh_T} \tag{5.3}$$

in which

Q = flow rate
A = gross cross-sectional area through which flow occurs
y = length of wetting from soil surface to wetting front during infiltration
h_T = constant total head loss in the transmission zone extrapolated to the wetting front = $h_o + h_c - h_w$
where:
h_o = constant depth of water on soil surface
h_c = constant capillary potential head at wetting front
h_w = constant pressure potential loss in wetting front in excess of transmission loss
t = time of infiltration

The relationship between the two dimensionless parameters y/h_T and tK/nsh_T of Equation (5.3) shown in a log-log plot is curvilinear as shown in Figure 4. The curvilinear relationships are represented by several straight lines.

Four consecutive straight lines were used to replace the curvilinear relationship between $y/h_T = 0.01$ and $y/h_T = 30$.

Four power equations showing y/h_T as a function of tK/nsh_T were developed from the straight line approximation.

For $0.1 \leq y/h \doteq < 0.1$

$$\frac{y}{h_T} = 1.45 \left(\frac{tK}{nsh_T}\right)^{0.5} \tag{5.4}$$

For $0.1 \leq y/h_T < 1$

$$\frac{y}{h_T} = 1.82 \left(\frac{tK}{nsh_T}\right)^{0.55} \tag{5.5}$$

For $1 \leq y/h_T < 5$

$$\frac{y}{h_T} = 2.19 \left(\frac{tK}{nsh_T}\right)^{0.68} \tag{5.6}$$

And for $5 \leq y/h_T < 30$

$$\frac{y}{h_T} = 1.83 \left(\frac{tK}{nsh_T}\right)^{0.85} \tag{5.7}$$

Instead of calculating the y/h_T for each infiltration problem for which these equations can be used, four times can be calculated to specify points at which the straight line approximations change. These typical times t_1, t_2, t_3, and t_4 for the separation of different infiltration flow periods can be obtained by substituting the values of y/h_T into the corresponding equations such that

For $y/h_T = 0.1$

$$t_1 = 0.00476 \frac{nsh_T}{K} \tag{5.8}$$

For $y/h_T = 1$

$$t_2 = 0.316 \frac{nsh_T}{K} \tag{5.9}$$

For $y/h_T = 5$

$$t_3 = 3.26 \frac{nsh_T}{K} \tag{5.10}$$

For $y/h_T = 30$

$$t_4 = 26.86 \frac{nsh_T}{K} \tag{5.11}$$

The length of the wetting from soil surface to the wetting front during infiltration can be calculated directly by rearranging Equations (5.4), (5.5), (5.6), and (5.7) by multiplying both sides by h_T. From this manipulation, four equations for the downward movement in soil are found.

For $t < t_1$

$$y = 1.45 \left(\frac{Kh_T t}{ns}\right)^{0.5} \tag{5.12}$$

For $t_1 \leq t < t_2$

$$y = 1.82 \left(\frac{Kh_T^{0.818} t}{ns}\right)^{0.55} \tag{5.13}$$

For $t_2 \leq t < t_3$

$$y = 2.19 \left(\frac{Kh_T^{0.47} t}{ns}\right)^{0.68} \tag{5.14}$$

For $t_3 \leq t < t_4$

$$y = 1.83 \left(\frac{Kh_T^{0.177} t}{ns}\right)^{0.85} \tag{5.15}$$

Infiltration in the horizontal direction is simpler because the component of gravity is zero and the water is drawn into the soil by matrix suction forces only. Many studies such as Green and Apt (1911) and Toscoz et al. (1965) have expressed the horizontal advance of the wetting front, x, as a function of $t^{1/2}$. Fok and his colleagues followed the derivation of Hansen (1955).

Darcy's Law states

$$Q_x = KA \frac{h_x}{x} \tag{5.16}$$

and the continuity equation is

$$Q_x = nsA \frac{dx}{dt} \tag{5.17}$$

where:

Q_x = horizontal flow rate
h_x = horizontal pressure head loss
x = lateral advance of wetting front
$ns = \delta\theta$ = incremental volumetric moisture content

Equating the two equations yields

$$KA\frac{h_x}{x} = nsA\frac{dx}{dt} \tag{5.18}$$

and integrating the equation leads to

$$x = \left(\frac{2Kh_x}{ns}\right)^{1/2} t^{1/2} \tag{5.19}$$

The model was placed into a computer program by Kim (1986). This program was written to include effects of a capillary fringe in the soil caused by a water table. Kim's program was revised for this study to include soils with or without a capillary fringe. The model, which is based on the concepts and theories developed by Fok and his colleagues, was programmed by Kim and has been modified by the authors; it will be referred to as "Fok's Model" throughout this report.

LABORATORY MODEL DESIGN AND CONSTRUCTION

The laboratory model consisted of three major parts; the soil compartment, tailwater compartment, and infiltration trench (Figure 5). The soil compartment held the soil medium that was to be tested. The tailwater compartment was used to establish a water table in the soil medium. The infiltration trench was simply an 8-inch wide and 28-inch long rectangular box to which water was added.

First, the size of the model had to be decided upon. Fok, Chung, and Clark (1982) used a box with a 27.6-inch width for a continuous line source of water supply. Yim and Sternberg's experiment (1984) used a 78-inch width for a trapezoidal trench with a 48-inch top width. These models did not experience any boundary effect from the side walls. The present laboratory model was constructed 56 inches wide and 48 inches high. The trench used in this model was 8 inches wide. The dimensions used in this model were considered acceptable.

The model was constructed of 3/4-inch thick A/C-grade plywood treated with a water sealer that prevented water from being absorbed into the wood. All joints in the tailwater compartment were sealed with a silicone caulk to prevent leakage. The edges of the soil and tailwater compartments were reinforced with corner brackets to prevent buckling. The tailwater compartment or outer box was constructed first and nailed to the bottom of the model. The inner box or soil compartment was then placed inside the outer box, centered and bracketed to the bottom of the model to keep it in place (Figure 6). The inner box was not caulked because water was to flow freely from the soil compartment to the tailwater compartment. The entire model was placed on cinder blocks to allow for easier drainage from the bottom valve.

The sides of the soil compartment had 1/4-inch holes drilled in a 1-inch grid to allow the water to flow freely from the soil compartment into the tailwater compartment. The sides of the soil compartment were lined with filter fabric to prevent the soil from moving into the tailwater compartment.

The tailwater compartment was used to establish a water table in the soil medium. The tailwater level or water table height could be controlled by six valves located at different elevations with 6-inch intervals around the sides of the box (Figure 7). All of the outlets were 1/2-inch valves.

The infiltration trench was constructed by building a frame and then stapling aluminum sheeting to the frame. The aluminum sheeting was punched with 1/16th-inch diameter holes in a 1/3-inch grid. This allowed the water to flow freely from the trench but at a uniform, controlled rate.

The water content, θ, at different locations in the soil medium was measured by soil moisture meters purchased from the SoilMoisture Equipment Corporation of Santa Barbara, California. These water contents were measured to track the flow of the water and the position of the wetting front in the soil medium. The soil moisture meter worked by measuring the resistance in ohms in the soil moisture block. The resistance corresponded to specific meter readings. Both the resistance and meter readings can be related to the soil suction in bars (Figure 8). For each soil in which the soil moisture meter and blocks were used, a graph could be produced relating the soil moisture meter readings to the water contents (Figure 9).

Therefore, the soil moisture meter readings had to be calibrated with the water contents of the soil being tested. This was done by placing a known volume of dry soil in a glass container. A small volume of water was then added to the container. From these volumes, the volumetric water content of the soil could be calculated. When the water was evenly distributed throughout the soil in the glass container, the soil moisture meter was read giving the corresponding reading to that specific water content. Evaporation of the water from the soil was prevented by sealing the container. This experiment was done twice for each soil to verify the results. From this data a graph was plotted for each soil relating the volumetric water content to the soil moisture meter readings.

Porosity of the soil was also found from the above experiment. Porosity is defined as the volume of voids to the total volume and is expressed as a decimal or percentage. When the soil became saturated, the volume of water was equal to the volume of voids and the porosity could be calculated.

Three different soils were tested in the laboratory model. The first was a concrete sand; the second, a clay loam; and the third, a loam. The permeability of the sand was measured with a falling head laboratory apparatus. The permeabilities of the clay loam and the loam were measured in the soil box with a Guelph Permeameter purchased from the SoilMoisture Equipment Corporation. The tests in both cases were run twice to verify the results. The Guelph Permeameter is an in-hole constant-head permeameter using the Mariotte Principle. The method involves measuring the steady-state rate of water recharge into the soil from a cylindrical well hole in which a constant head of water is maintained (Figure 10). Constant head in the well hole is established by regulating the level of the bottom of the air tube. As the water level in the reservoir falls, a vacuum is created above the water and is relieved when air bubbles emerge from the air inlet tip and rise to the top of the reservoir. When a constant well height of water is established, a bulb of saturated soil is created (Figure 10). The shape of the bulb is numerically described by a C factor as shown in Figure 11. Once the bulb is established, the outflow of water from the well reaches a steady-state flow rate that can be measured. The outflow rate, diameter of the well and height of

water in the well are used to determine the hydraulic conductivity or permeability by these equations:

$$K = G_2Q_2 - G_1Q_1 \tag{6.1}$$

where

$$G_2 = \frac{H_1C_2}{\pi[2\,H_1H_2\,(H_2 - H_1) + a^2\,(H_1C_2 - H_2C_1)]} = 0.0041 \tag{6.2}$$

$$G_1 = G_2\frac{[H_2C_1]}{[H_1C_2]} = 0.0054 \tag{6.3}$$

$$Q_1 = (X)(R_1) \text{ or } (Y)(R_2) \tag{6.4}$$

$$Q_2 = (X)(R_2) \text{ or } (Y)(R_1) \tag{6.5}$$

in which

K = hydraulic conductivity in cm/sec
H_1H_2 = well height for first and second measurements, respectively, in cm
C_1C_2 = C factors corresponding to H_1/a and H_2/a, respectively
a = well radius in cm
X = 35.8 cm^2 = reservoir constant used when the inner reservoir only is selected, expressed in cm^2
Y = 2.14 cm^2 = reservoir constant used when the inner reservoir only is selected, expressed in cm^2
R_1R_2 = steady-state rate of fall corresponding the H_1 and H_2, respectively, and converted to cm/sec

For the clay soil, the inner reservoir only was selected and the equation becomes

$$K = (0.0041)(2.14)(R_2) - (0.0054)(2.14)(R_1) \tag{6.6}$$

The readings R_1 and R_2 were found at 5-cm well head height (H_1) and 10-cm well head height (H_2), respectively.

A sieve analysis of each soil was performed according to the American Society of Testing Materials (ASTM) standards. The sieve analysis aided in the classification of the soils according to the triangular soil classification chart developed by the U.S. Department of Agriculture.

After the soil properties had been tested, the infiltration trench experiment was ready to be run. The soil was placed in the box and the soil moisture blocks were layered in a grid. The trench was then placed in the center of the soil compartment and the experiment was begun.

EXPERIMENTAL RESULTS AND COMPARISON WITH NUMERICAL MODELS

I. Sand Experiments

The first laboratory experiments were run with a coarse construction sand as a medium. The sand was placed in the soil compartment in layers up to a total depth of 37 inches. A sieve analysis was performed on the soil with the resulting grain size distribution curve shown in Figure 12. From this graph, the median particle size, D_{50}, and the coefficient of uniformity, C_u, were found to be 0.6 mm and 3.5 mm, respectively. The sand was evenly compacted by leveling when the soil moisture blocks were placed in layers. The sand was used for a few trial experiments to gauge how much water should be used and at what rate. Soil moisture blocks were arranged in six rows which were placed 6 inches apart and in seven columns that were 3-1/2 inches apart. The upper two rows contained only five columns because the trench was imbedded in the sand to a depth of 8 inches and the two middle columns were directly beneath the trench (Figure 13). A water table was established in the sand at a depth of1 foot above the bottom of the soil compartment.

The soil moisture blocks were calibrated with the sand as described previously. The water content versus meter readings graph is shown in Figure 14. From this same experiment, the porosity was found to be 35 percent. The permeability of the sand was determined in the soils laboratory using a falling head permeameter and was determined to be 0.945 inches per minute.

A capillary fringe formed in the sand just above the water table. The measured initial condition of the sand before water was added to the infiltration trench is compared with the initial condition predicted by the finite element model as shown in Figure 15. The authors found the agreement to be excellent.

The equal water content line of $\theta = 0.2$ is plotted and compared with the finite element model results (Figures 16 and 17). In the sand, the water did not travel a great distance horizontally. The wetting front simply merges downward to the capillary fringe after 10 minutes of the experiment and the water moved rapidly downward.

A second experiment was run in the sand to check whether the results could be duplicated (Figures 18 and 19). Both of these experiments were run with 4 inches of water in the infiltration trench which was allowed to infiltrate the sand. Results in the second experiment were similar to those in the first. The water infiltrated the sand quickly and the wetting front did not move a great distance in the horizontal direction.

These experiments show that sand is a good medium for an infiltration trench facility because the runoff would drain through it quickly. This occurs because of the sand's high permeability. However, the sand experiments did not produce a clearly defined wetting front, which made comparison with the computer models more difficult.

The Fok's model computer program was run with the initial soil moisture condition in the sand due to the established water table and the following soil parameters: permeability, K = 0.945 inches per minute and porosity, n = 0.35. The head loss, h, was found in Panikar (1977). An h = 4.25 inches was used.

It was difficult to compare Fok's model to the sand experiments because the model could not simulate the initial condition. Also, the permeability of the sand was so high that the time limit (t_4) in Equation (5.11) for the sand was 28 minutes. Fok's model also predicted movement in the vertical direction much greater than the lower boundary limits of the soil compartment. For this reason, the Fok's model results are not compared with the lab results in the figures. It can be concluded from these experiments that Fok's model is not accurate for sands.

The finite element results agreed with the experimental results. This model seems to be a good predictor of infiltration.

II. Clay Experiments

The clay was obtained from a construction site on the Virginia Tech campus. Permeability was tested in the soil box with the use of a Guelph Permeameter and was determined to be 3×10^{-3} inches per minute. The clay was calibrated with the soil moisture blocks, resulting in a graph of water content versus the meter readings (Figure 20). A sieve analysis was performed on the clay to classify the soil. The grain-size distribution curve of the clay is shown in Figure 21. Using the triangular soil classification chart, the clay was classified as a clay loam.

The clay was sifted through a screen with 1/4-inch square hole size. This was done to prevent the larger clumps of soil from being placed into the soil compartment because it was probable that clumps would interfere with even propagation of the wetting front.

The clay was placed in the soil compartment in layers up to a total depth of 28.5 inches. The trench was placed on top of the clay and embedded to a 1/2-inch depth. No water table was established in the soil compartment.

The clay was evenly compacted by leveling when the soil moisture blocks were placed in rows. The soil moisture blocks were placed in four rows. The lower row

was placed one foot from the bottom of the model. The lower three rows were placed six inches apart and the top two rows were three inches apart as shown in Figure 22. A water table was not established in these experiments because there was not enough depth to establish the capillary fringe zone. Without the water table, it would also be easier to see the wetting front develop. The clay was dry when placed in the box with an overall water content of zero.

The first experiment in the clay produced a well-defined wetting front. The experiment took a day to run because the wetting front moved slowly through the clay. The experiment was run with one inch of water in the trench, which was kept constant throughout the experiment. The clay experiment was run with less water in the trench than the sand experiment. This was done because the permeability of the clay was so much less than the permeability of the sand. The wetting front developed more slowly so that the computer models could be better tested against the laboratory results.

The results of the first experiment are shown in Figures 23 and 24. The results of the first experiment compared well with the predictions of Fok's model. For Fok's model, a porosity of 48 percent and a permeability of 0.003 inches per minute were used based on the laboratory test results. An h of 10.3 inches was used and was found from Panikar (1977). Fok's model was a good predictor of the propagation of the wetting front in both the horizontal and vertical directions. The first experiment results also compared well with the finite element model results.

The second clay experiment was run in the same manner. The results of the second experiment are shown in Figures 25 and 26. The results were a little different in that the wetting front moved more in the horizontal direction. A possible reason could be that the clay, after the first experiment, had to be dried and crushed and then placed back into the box. The finest particles of the soil were placed on top of the soil medium and, therefore, the water could move more easily in the horizontal direction instead of the vertical direction. The results of the second experiment were also well in line with Fok's model results.

Both experiments compared well with the finite element model predictions. The computed and measured fluxes were very close. The measured flux was 0.5 in^2/min and the computed flux was 0.45 in^2/min. Both Fok's model and the finite element formulation appear to be good predictors on infiltration in clay.

III. Loam Experiments

A topsoil was obtained from a construction site in the town of Blacksburg, Virginia. The permeability of the soil was tested in the soil box with the use of a Guelph Permeameter and was determined to be 0.007 inches per minute. The top soil was calibrated with the soil moisture blocks resulting in a graph of water

content versus the meter readings (Rigure 27). A sieve analysis was performed on the topsoil to classify the soil. The grain-size distribution curve of the topsoil is shown in Figure 28. The topsoil was classified as a loam, using the triangular soil classification chart.

The loam was sifted through the same screen used for the clay. The loam was placed in the soil compartment in layers up to a total depth of one foot eleven inches. The trench was placed on top of the clay and embeded to one-inch depth. The loam was evenly compacted by leveling when the soil moisture blocks were placed in four rows. The bottom row was placed six inches apart and the top two rows were three inches apart as shown in Figure 29. A water table was not established in the loam experiment because the depth of the loam was too shallow. The loam had an average water content of 8 percent when the experiment was begun. Only one experiment was performed on the loam.

The loam experiment, like the clay experiments, produced a well-defined wetting front. The experiment was run for 130 minutes. The wetting front in the loam moved more quickly than that of the clay and more slowly than that of the sand. The experiment was run with one inch of water in the trench and the water level was held constant throughout the experiment. The results are shown in Figures 30 and 31.

The loam experiment compared relatively well with Fok's model. An h of 13.06 inches was used and found from Panikar (1977). The vertical propagation of the wetting front was predicted well by Fok's model for 60 minutes. It did not predict the horizontal propagation as well. After 70 minutes, Fok's model results exceeded the limits of the laboratory model and are not shown on the figures.

The loam experiment also compared well with the finite element model predictions. Like Fok's model, the finite element model predicted wetting front movement beyond the soil box boundaries at around 70 minutes. For this reason, both results of Fok's model and the finite element model are compared with the laboratory model results up to 60 minutes.

PARAMETRIC STUDIES

Based on the comparison with the three numerical models and the laboratory tests, the finite element model developed in this study has been well verified. Its utility will be demonstrated by simulations for variably saturated flow problems. It provides the necessary tool to study the behavior of water movement from an infiltration trench to its surrounding porous medium.

To find the storage of water in the trench, routing is performed based on the following continuity equation.

$$\frac{dS}{dt} = I - O \tag{8.1}$$

where

dS/dt = rate of change of storage S in the trench
I = inflow
O = outflow across the trench boundary into the surrounding porous media.

Equation (8.1) can be written in the finite difference form.

$$\frac{S_2 - S_1}{\Delta t} = \frac{I_2 + I_1}{2} + \frac{O_2 - O_1}{2} \tag{8.2}$$

where subscripts 1 and 2 refer to the previous and current time levels.

Before the soil at the trench bottom is saturated, the boundary condition is the specified flux, which is equal to the inflow to the trench. In this case, all inflow infiltrates the soils. The routing is actually not required because there is no storage in the trench. The routing procedure is outlined:

Step 1. Assume a value for $h(x_B,y_B,t)$
Step 2. Compute O_2 through finite element analysis
Step 3. Compute S_2 by Equation (8.2)
Step 4. Compute water level based on trench geometry
Step 5. Check water level (computed $h(x_B,y_B,t)$ against assumed value for h(xb,yb,t)
Step 6. If the difference beween the computed and the assumed $h(x_B,y_B,t)$ is negligible, go to the next time step. If the difference is not negligible, go to Step 1.

I. Soil Properties

To study the effects of soil properties on infiltration, the finite element model has been applied to an infiltration trench, subjected to a given inflow hydrograph, but for several different soils. The geometry of the trench and the boundary conditions prescribed are shown in Figure 32. Soil properties are defined by van Genuchten's model. The values used in the model are listed in Table 1 (Carsel and Parrish 1988).

A wide variety of soils has been examined, ranging from silty clay to sand. The time steps used are 0.25 min. for sandy soil, 0.50 min. for loamy soil, and 1.00 min. for silt and clay. Water table is fixed at a depth 8 feet below the bottom of the trench. Initial water content varies for each type of soil. The simulation results are shown in Figures 33 and 35. The inflow hydrograph to the trench is shown in Figure 33. The outflow due to infiltration from the trench to surrounding soils is shown in Figure 34 for different soils. The change of water level in the trench for different soils is shown in Figure 35.

One observation from those results is that the saturated conductivity K_s and parameter λ in van Genuchten's model are the most important factors in this infiltration study. It has been shown from their model that large K_s and small λ will yield a high infiltration rate. Large K_s is usually associated with large λ. Infiltration rate is not simply proportional to the saturated hydraulic conductivity, but rather to the ratio of K_s/λ. Soils having large values of K_s/λ give high infiltration rate and therefore the water levels in the trench are lower.

II. Geometries

The effects of geometries of the trenches on infiltration have been studied. A deep, narrow trench is compared to a wide, shallow one for the same inflow hydrograph, trench length, and soil type. Sandy loam and loam are examined in this study. Keeping the total trench volume constant, deep trenches give a higher infiltration rate because of the increase of pressure head due to high water depth in the trench. However, wide trenches give higher infiltration volume due to the large horizontal area through which vertical infiltration takes place. Both the width and depth of the trench play important roles in the determination of infiltration volume.

Figures 36 and 37 show that wide, shallow trenches give a higher infiltration rate initially and approach the same steady-state infiltration rate. Comparison has also been made for the two trenches which have the same input hydrograph and trench depth but are different in length and width. The trench volume remains constant. Results shown in Figures 38 and 39 indicate that the short, wide trench has a higher infiltration rate and lower water level in the trench than the long, narrow trench.

III. Water Tables

Because of the capillary effect, the location of the water table will determine the initial water content distribution. For different soils, the effects of the water table location vary. The model is applied to a one-foot long, one-foot deep, and two-foot wide trench filled with water all the time. The infiltration rates at the end of the first minute have been computed for different water table locations. Results for different soils with a change of water tables from three foot to 80 foot are shown in Figure 40. There exists a limit for each soil beyond which the water table has no effect on infiltration. The limit is defined as the depth at which change in infiltration rate is less than one percent of the infiltration rate at the previous depth. The limit for sand is about 10 feet; 30 feet for loamy sand; and 60 feet for sandy loam.

IV. Effects of Sediment Deposition in Trench

Sediment deposition will reduce the permeability on the trench bottom. A 3-inch thick sediment layer is assumed with 75 percent, 50 percent, and 25 percent of the original permeability, respectively. Using the same trench geometry and inflow hydrograph as shown in Figures 32 and 33, routings are performed for a sandy loam soil. The results are shown in Figure 41. There are obvious reductions in infiltration rate before the maximum water level in the trench is reached. After this point, the differences become small in infiltration rates for reductions in permeability which are less than 50 percent.

V. Distribution of Water Content

A 2,000-minute infiltration process has been simulated to examine the movement of the wetting front due to the rising and falling of water level in the trench during a storm event. The trench geometry shown in Figure 32 and the inflow hydrograph shown in Figure 33 are used. The soil chosen for this simulation is loam. In figures 42 and 43, the advancing of the wetting front due to soil moisture movement and the change of water levels in the trench are shown using the results predicted by the finite element model.

CONCLUSIONS

In this study, a two-dimensional finite element model has been developed to simulate the transient flow of water in a variably saturated porous medium. The model simulates pressure heads and moisture distributions in the soils surrounding an infiltration facility and fluxes across the boundaries of the facility. Routing has also been performed to find the infiltration rate, water depth, and storage in the facility, and any overflow that may occur.

Governing equations have been derived and placed into a finite element analysis to arrive at the finite element formulation. The finite element model has been verified for one-dimensional transient vertical flow by comparison with van Genuchten's finite element model. It has also been verified for two-dimensional transient flow by comparison with the Selim and Kirkham model. Lastly, the model has been verified for steady-state flow through a square embankment by comparison with the results predicted by Huyakorn et al.

The results of the finite element formulation and an infiltration model developed by Fok et al. have been compared with the results of laboratory model study. Fok's model is a two-dimensional infiltration model for furrow irrigation expressed in explicit form. Vertical and horizontal advances of the wetting front are calculated based upon Darcy's Law and the principle of continuity. The laboratory model was designed to test infiltration trenches specifically and used soil moisture blocks to measure the water contents in a grid pattern within the soil being tested. Three soils were tested. The results of soil moisture distribution compared well with the predictions of the finite element model for all three soils. In this study, Fok's model was not accurate for the sand, but was reasonably accurate for the clay and the loam. The finite element formulation developed in this study has been well verified by comparisons with other numerical models, Fok's infiltration model, and laboratory tests.

Parametric studies have been performed with the finite element model for loam soil and sandy loam to determine the various effects of such parameters as soil properties, facility geometries, and depth of water tables. Sands are recommended for use in an infiltration facility while clays are not. Saturated soil conductivity and the λ parameter from van Genuchten's model are found to have the greatest effect on infiltration rate. Where geometry is concerned, a wide, shallow trench is recommended for a given trench length and trench volume. A short, wide trench is recommended for a given depth and trench volume. The depth of the water table has been shown to have a greater effect in silt than in sand. There exists a limit for each soil beyond which the water table has no effect on infiltration. The limit for sand is about 10 ft.; 30 ft. for loamy sand; and 60 ft. for sandy loam.

In the design of an infiltration trench, geometries vary considerably and water depth in the trench varies with time. The water flux across the bottom and sides of the trench is an important factor in sizing the trench. The finite element formulation has the capability to change geometries and is a useful tool in the design of infiltration facilities to calculate the flux and water level in the trench.

FIGURES

FIGURE 1
Comparison of Finite Element Model with van Genuchten's Model

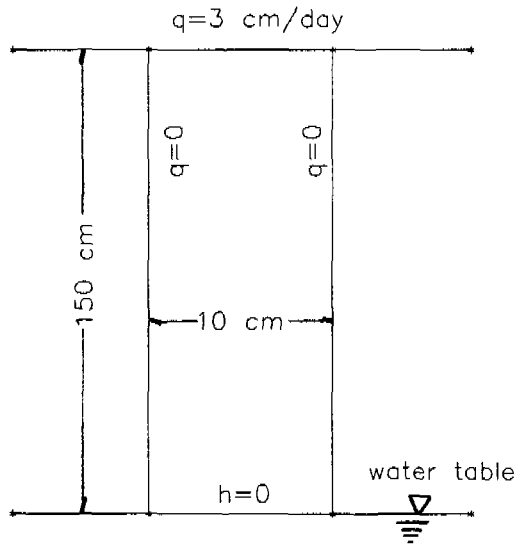

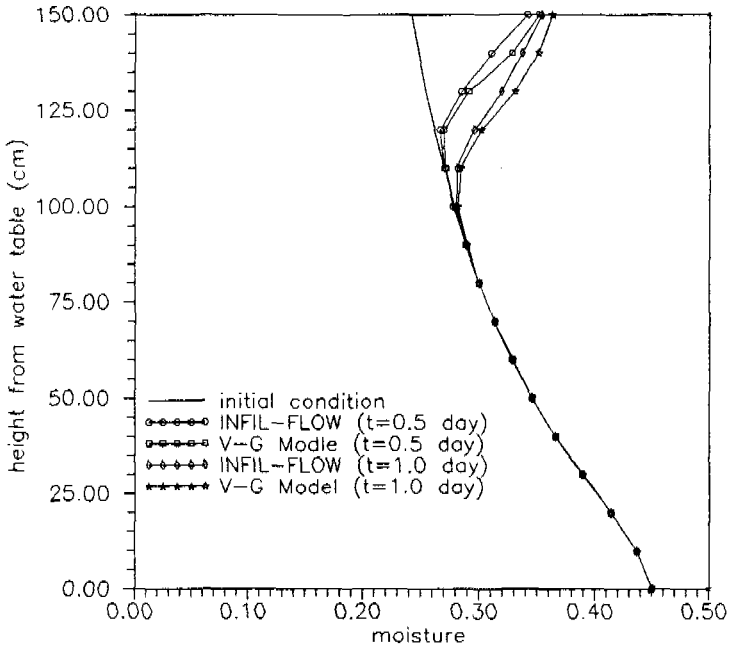

FIGURE 2
Comparison of Finite Element Model with Selim and Kirkham's Model

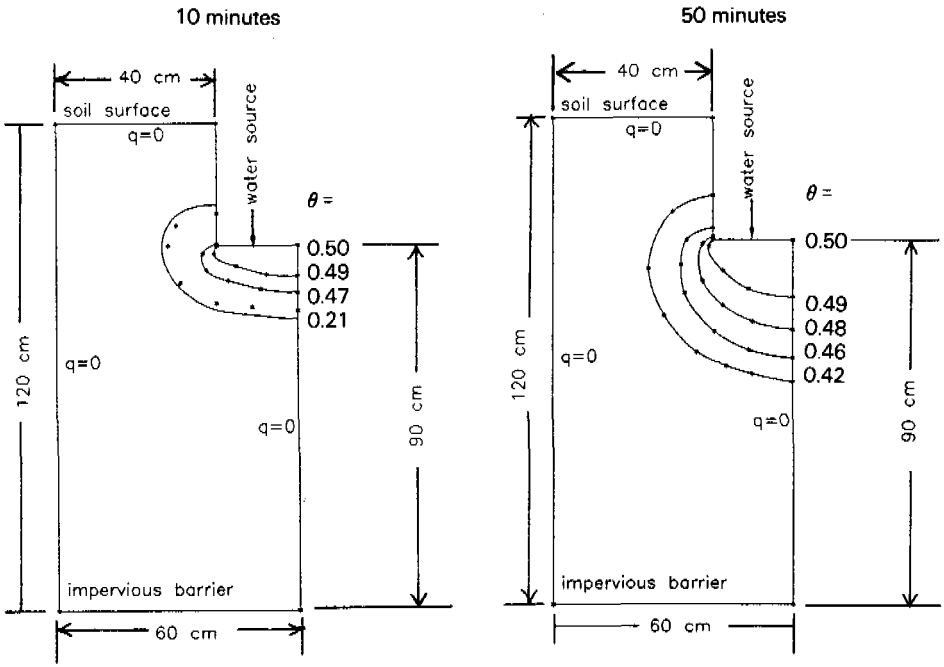

. . . . Selim and Kirkham's Model
—— INFIL-FLOW

FIGURE 3
Comparison of Finite Element Model with Huyakorn's Model

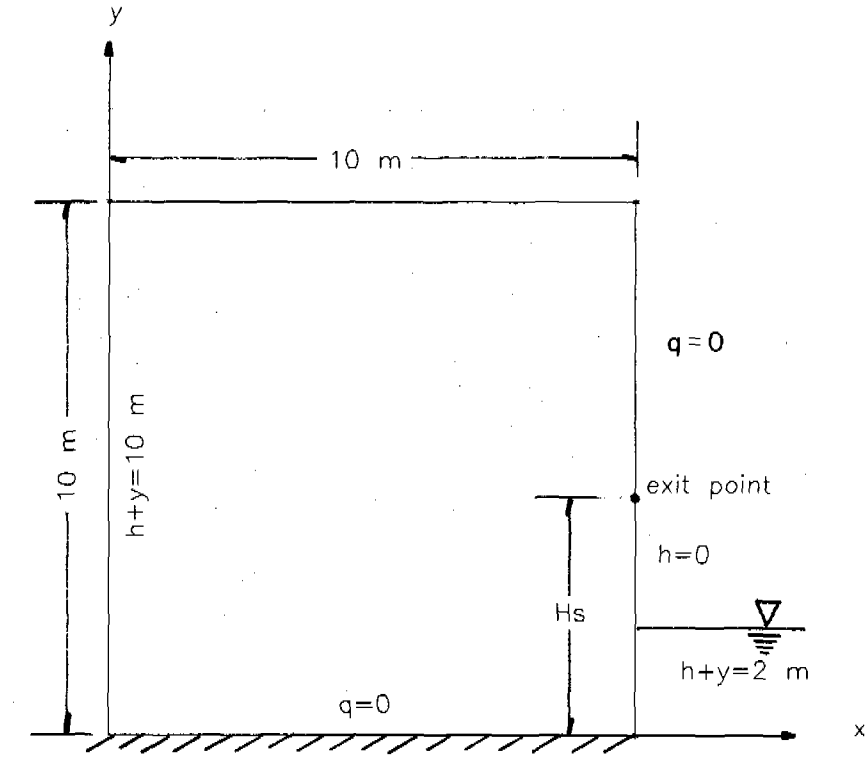

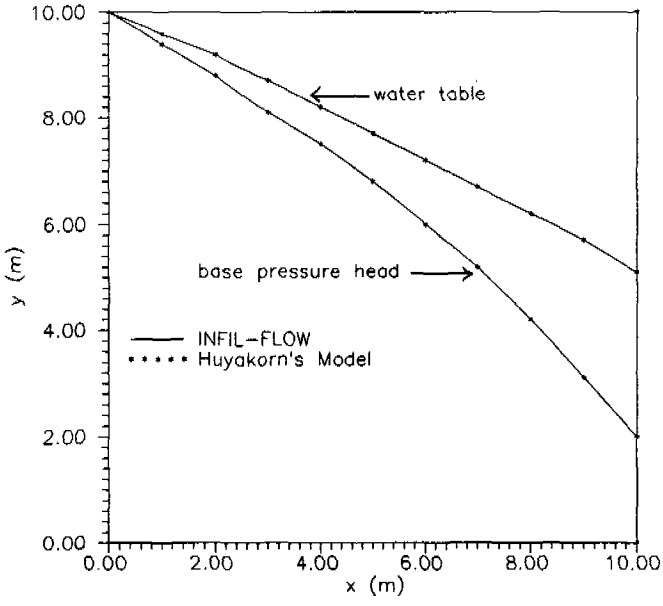

FIGURE 4
Relationship between y/h and Kt/nsh
(Fok et al. 1982)

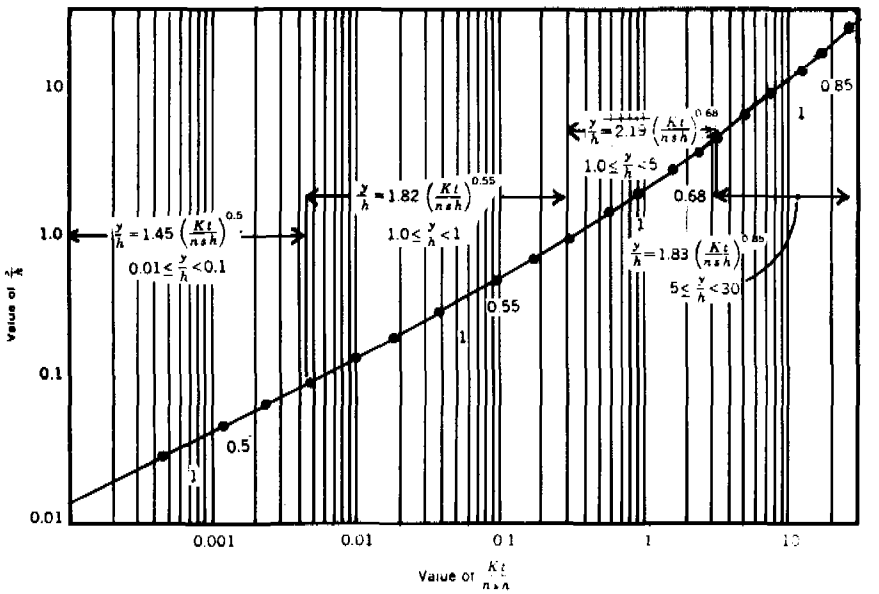

FIGURE 5
Top View of Laboratory Model

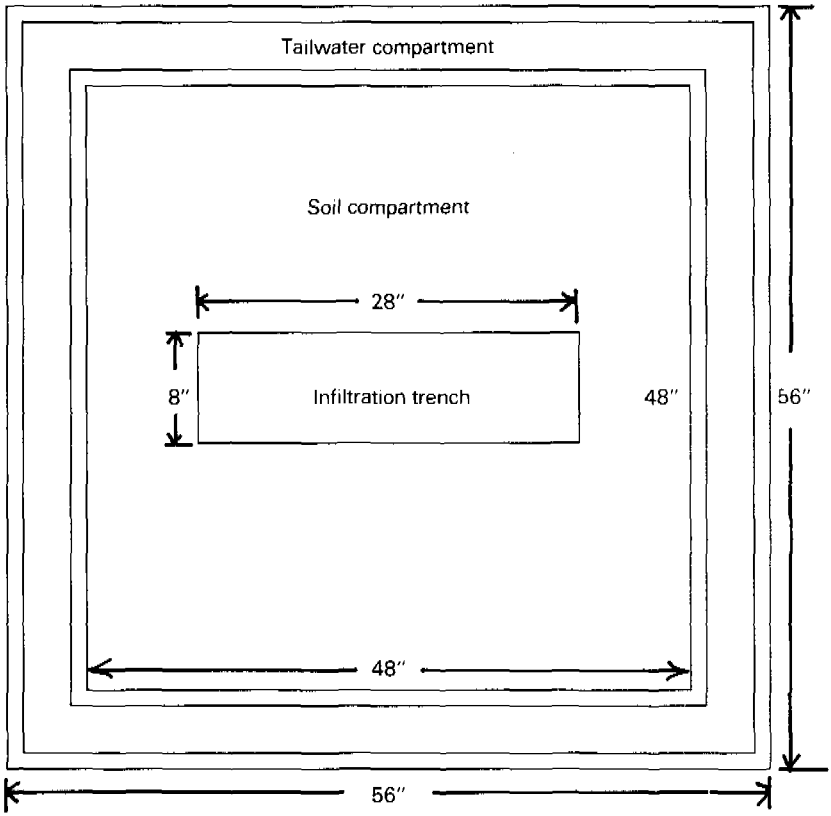

FIGURE 6
Three-dimensional View of Laboratory Model

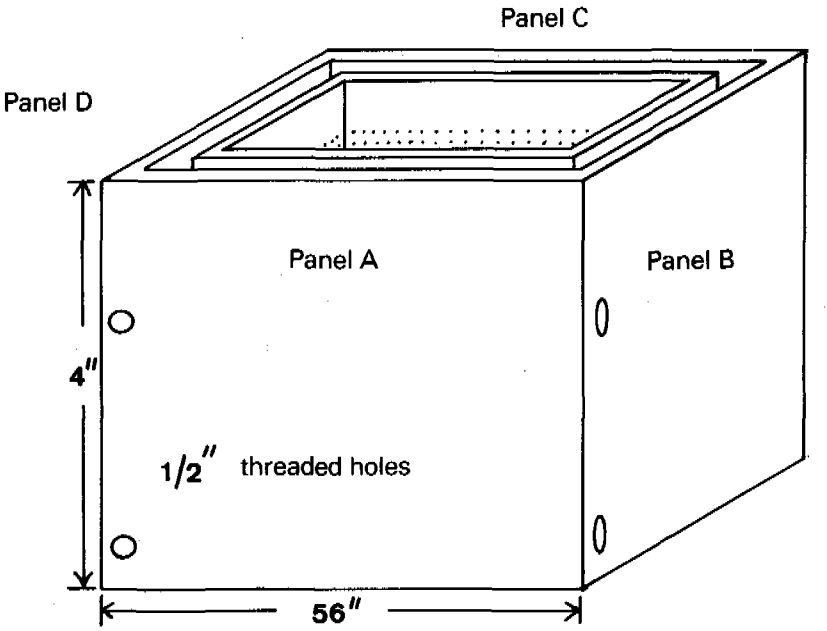

FIGURE 7
Panels of Tailwater Compartment with Outlets

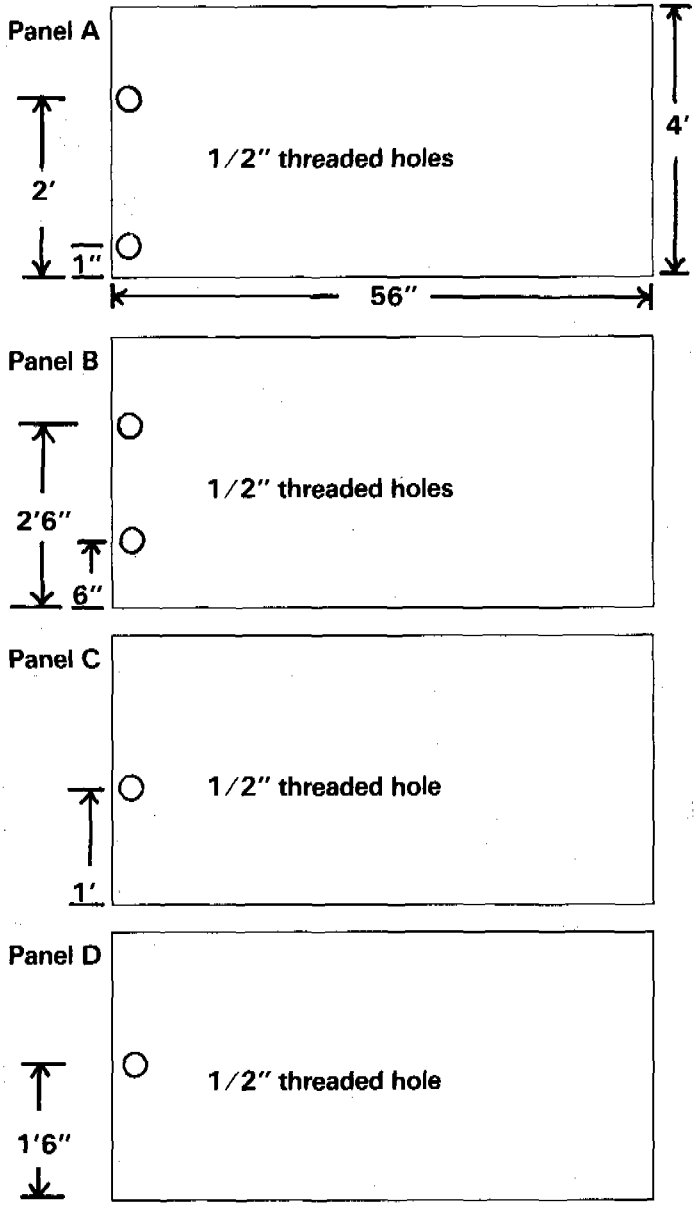

FIGURE 8
Relationship of Meter Readings to Soil Suction
(SoilMoisture Equipment Corp. 1985)

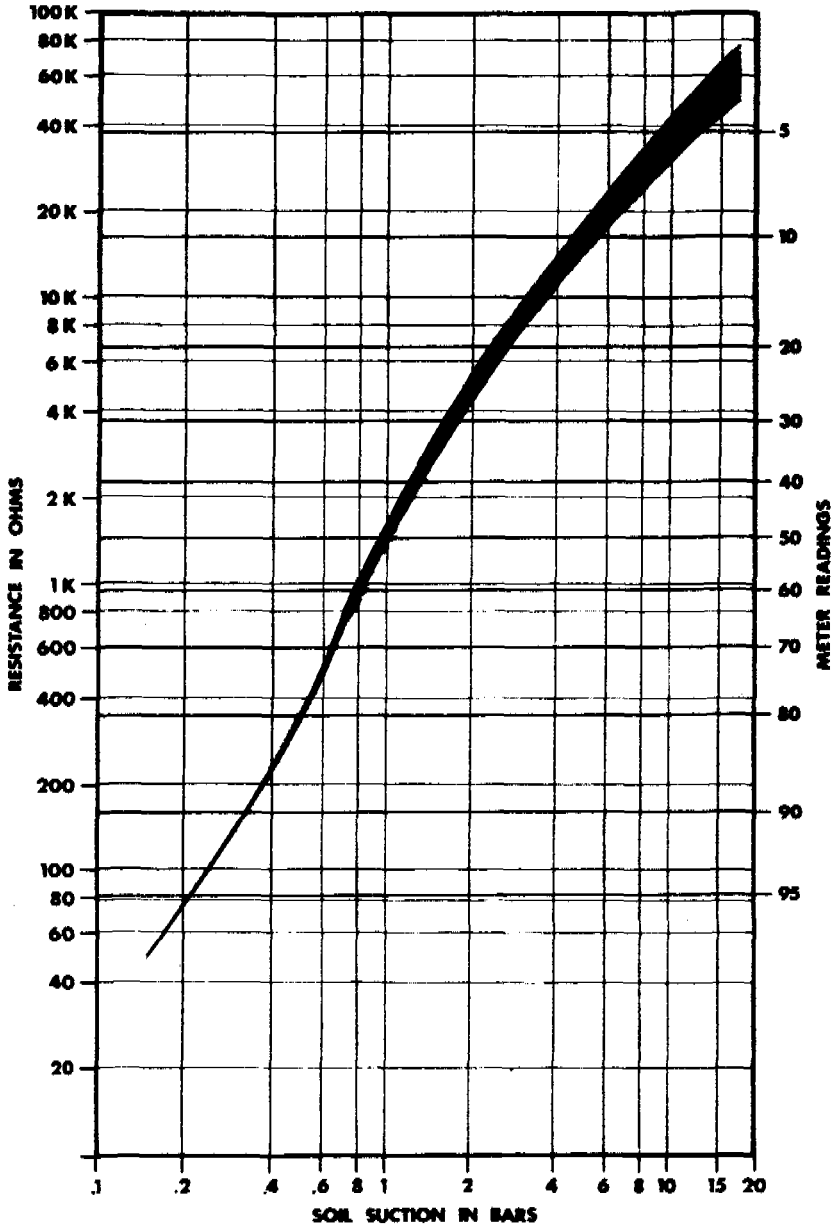

FIGURE 9
Relationship of Meter Readings to Water Content
(SoilMoisture Equipment Corp. 1985)

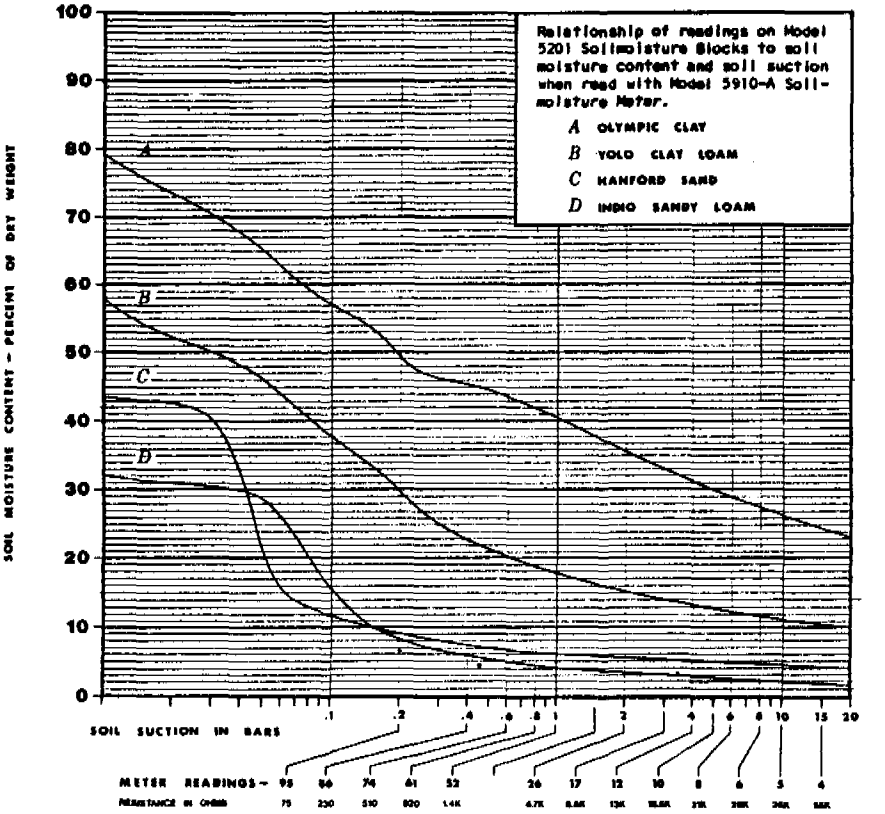

FIGURE 10
Guelph Permeameter
(SoilMoisture Equipment Corp. 1986)

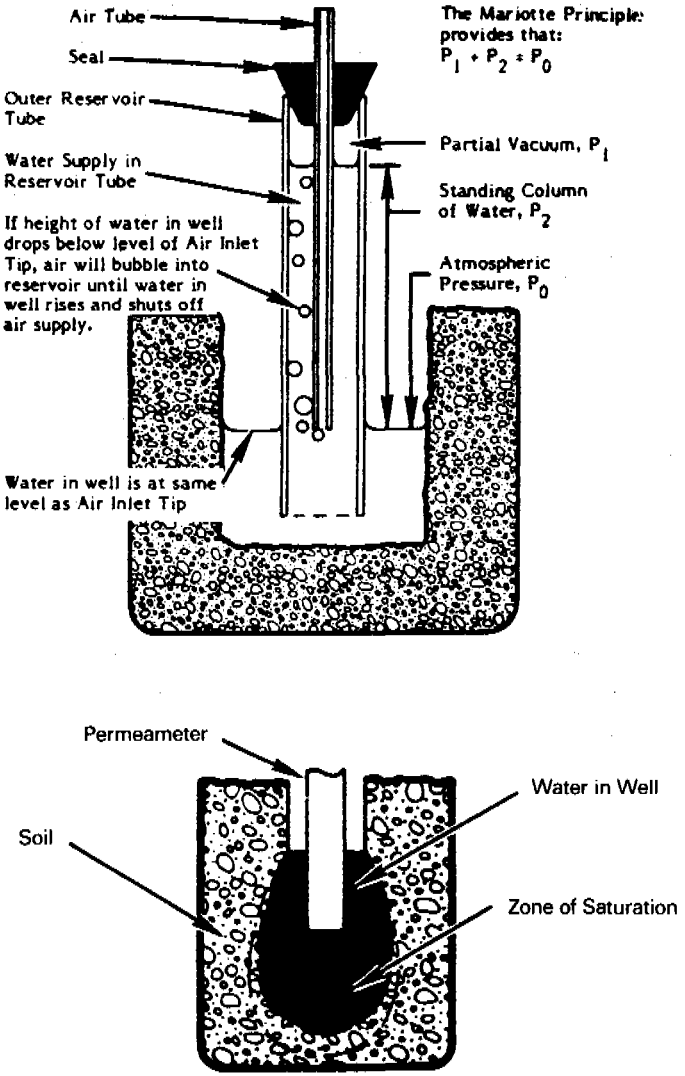

FIGURE 11
C Factor for Guelph Permeameter
(SoilMoisture Equipment Corp. 1986)

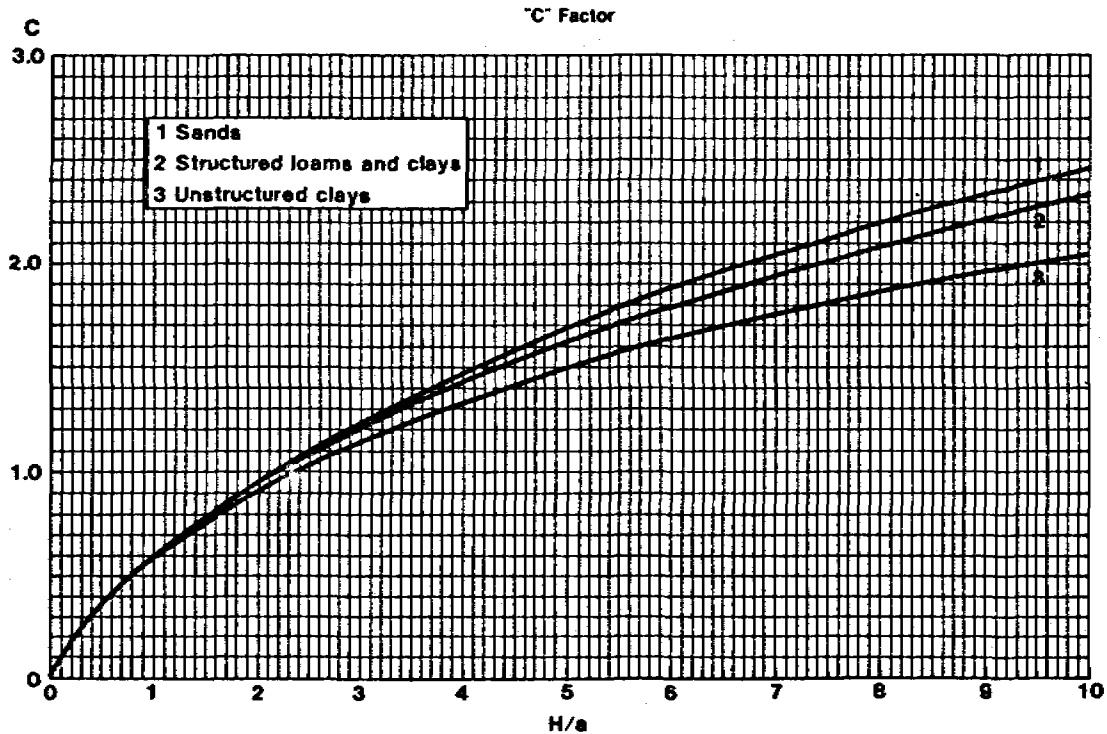

FIGURE 12
Grain Size Distribution Curve of Sand

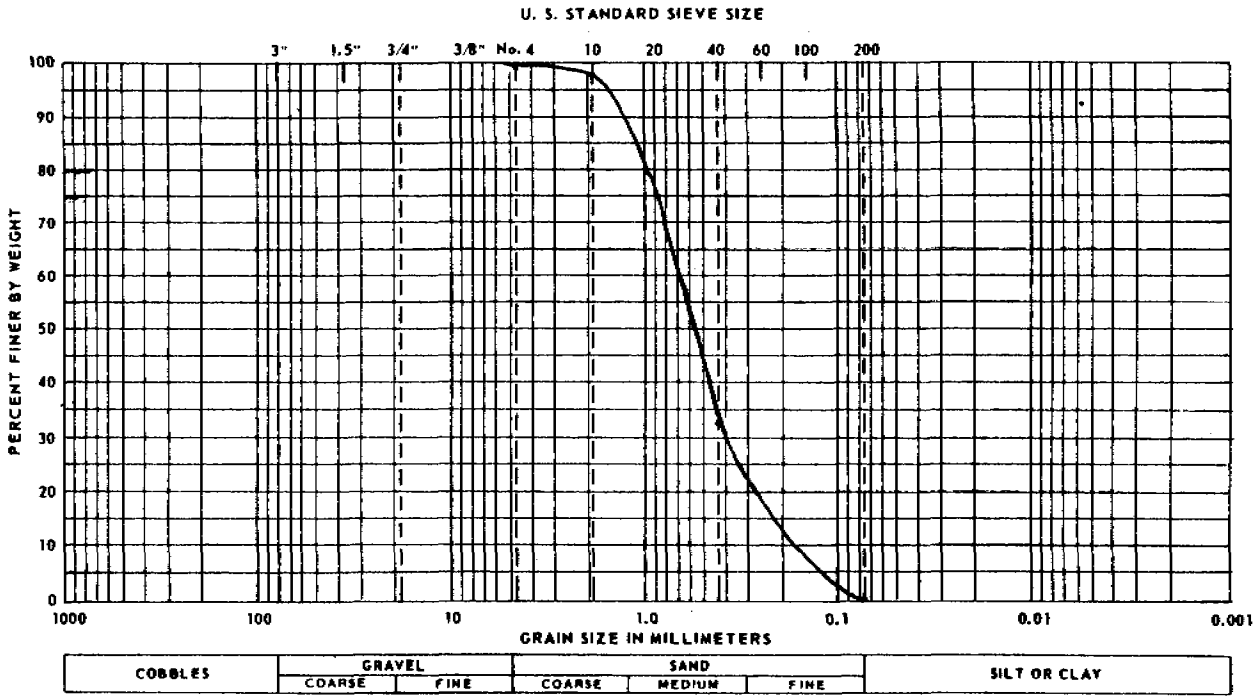

FIGURE 13
Placement of Soil Moisture Blocks in Sand

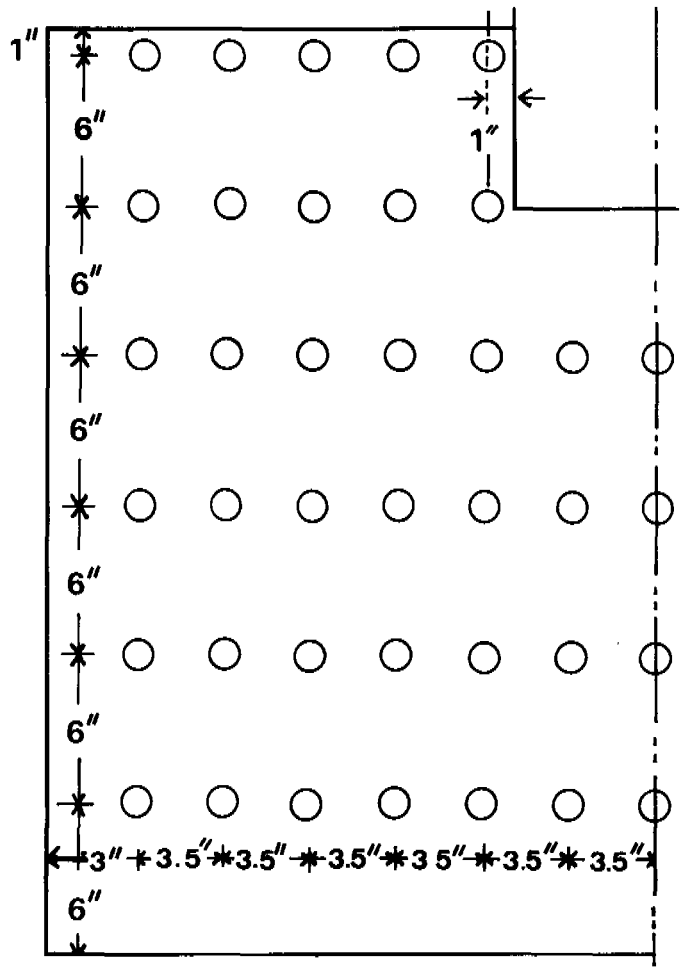

FIGURE 14
Water Content versus Meter Readings for Sand

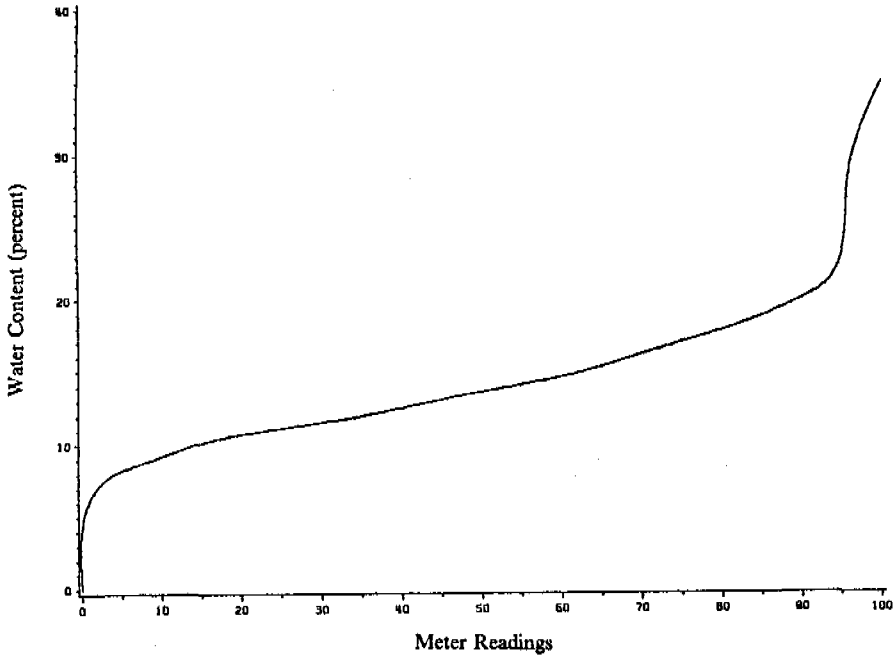

FIGURE 15
Initial Moisture Condition for First Sand Experiment

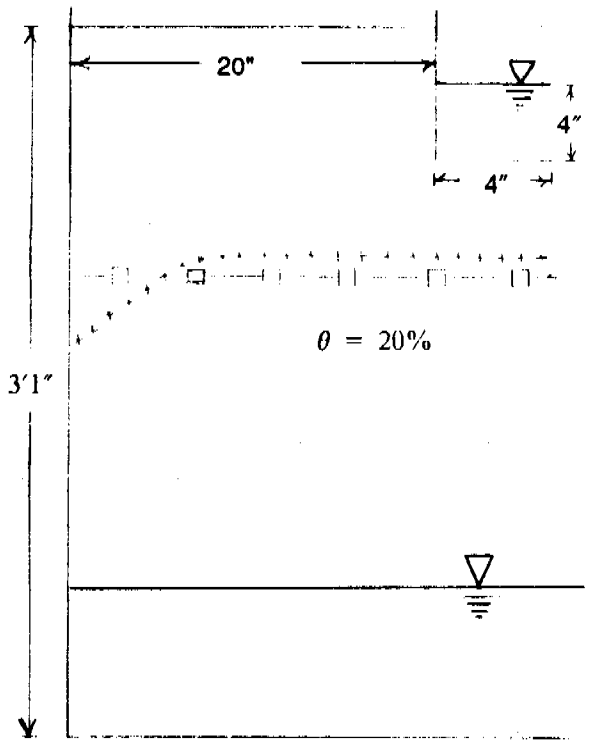

FEM —□—□—

measured + + + + + +

FIGURE 16
Results of First Sand Experiment (10 and 30 Minutes)

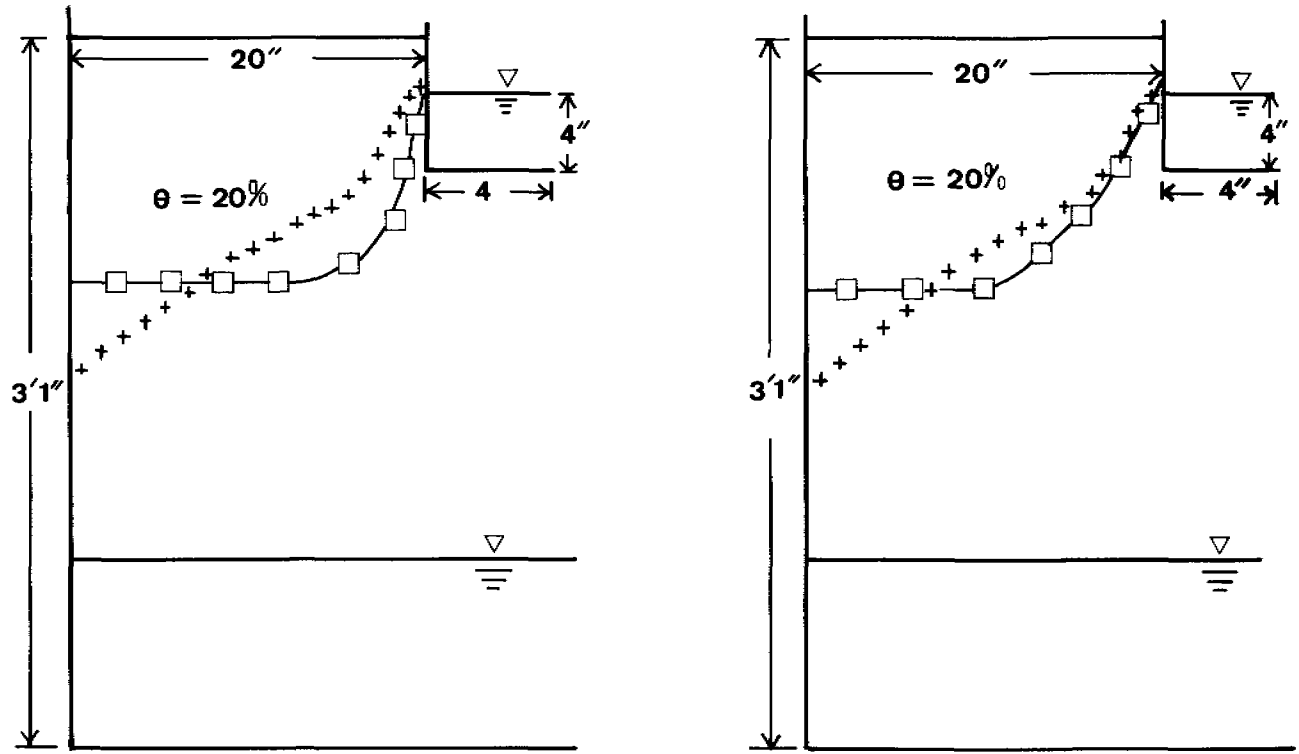

FIGURE 17
Results of First Sand Experiment (50 and 100 Minutes)

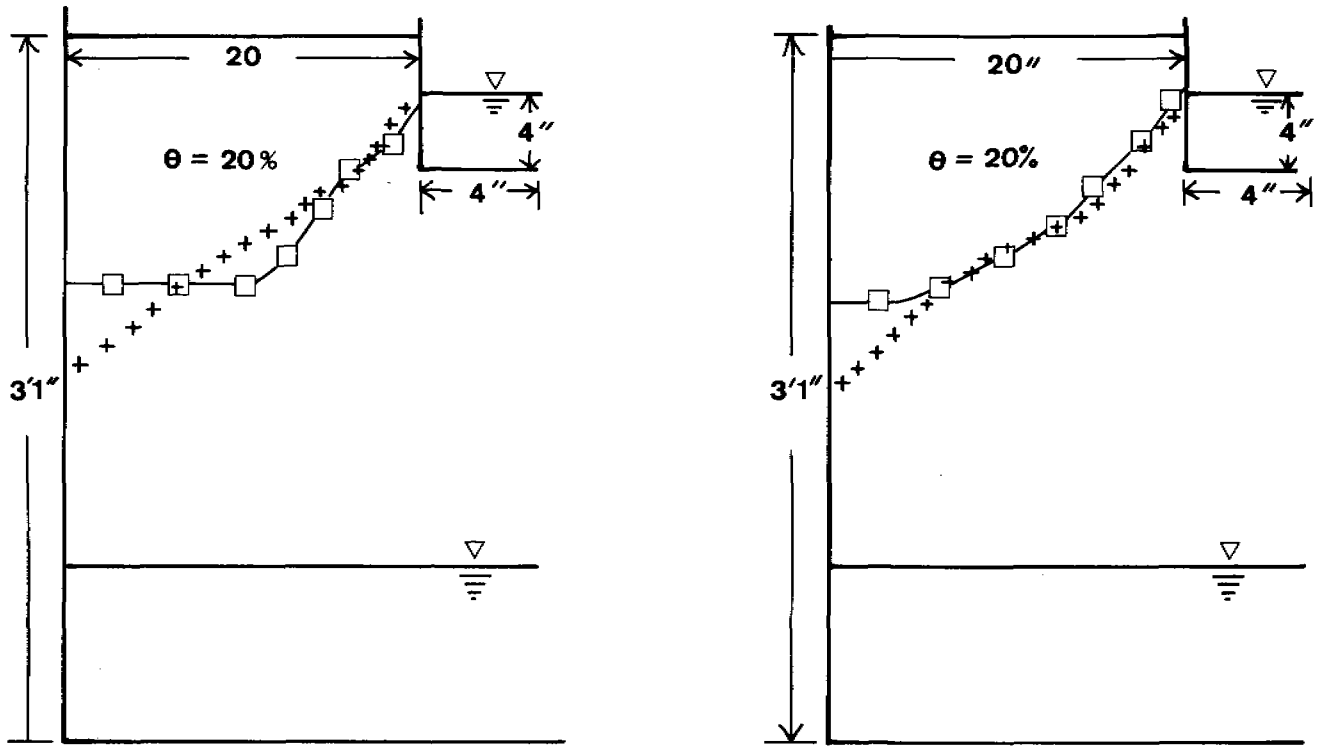

FIGURE 18
Results of Second Sand Experiment (Initial Condition and 20 Minutes)

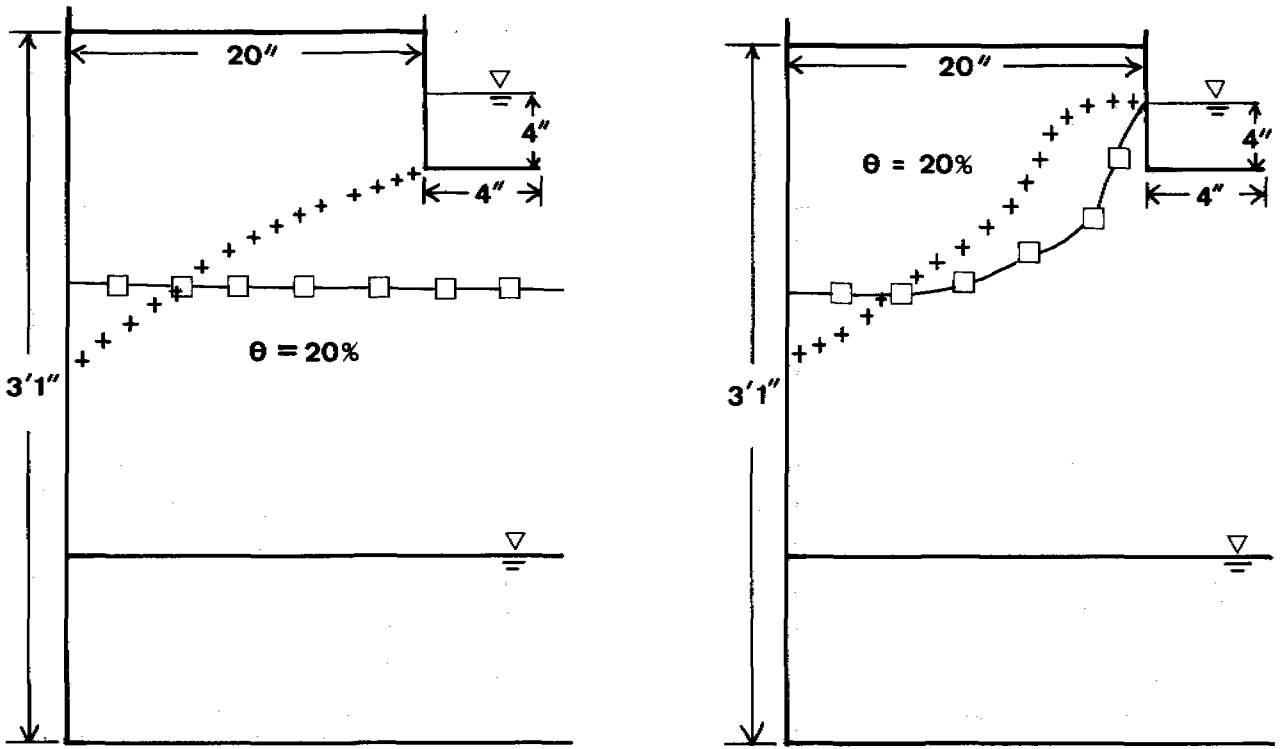

FIGURE 19
Results of Second Sand Experiment (50 and 100 Minutes)

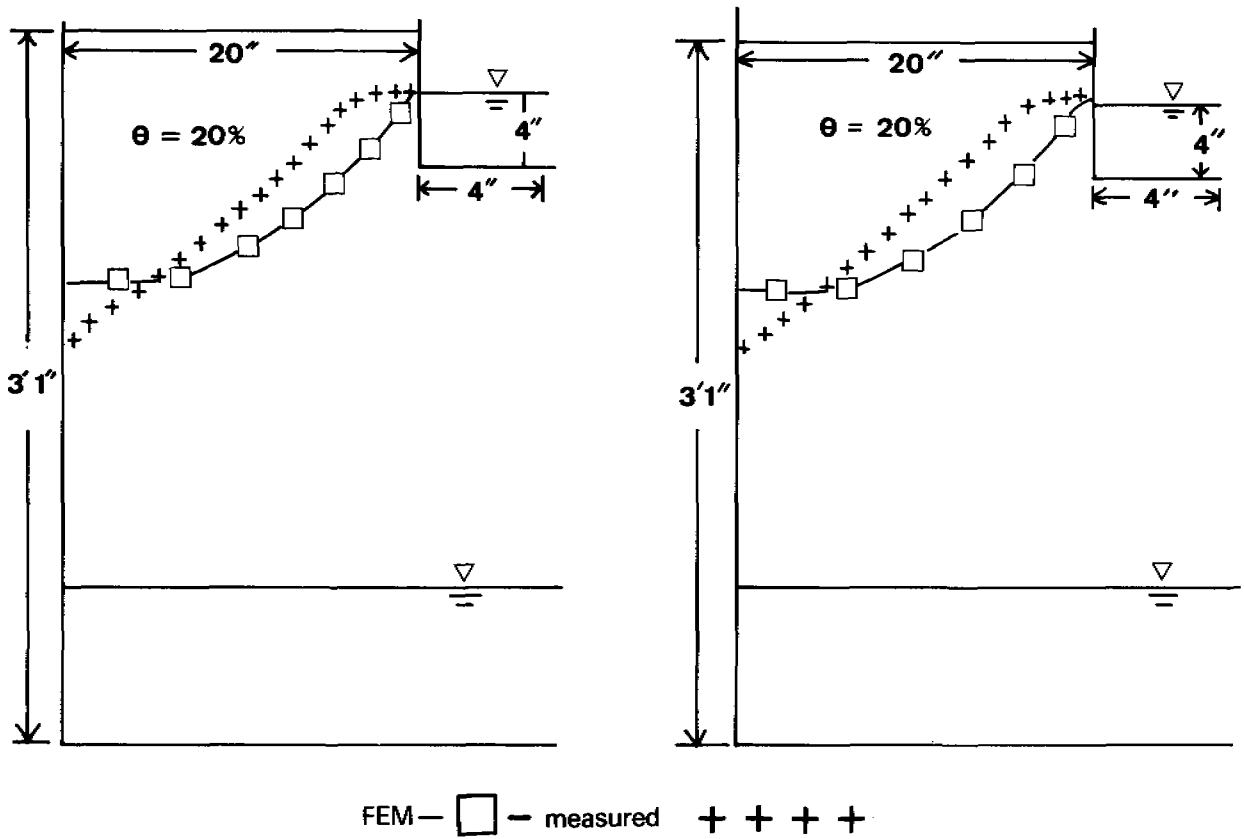

FIGURE 20
Water Content versus Meter Readings for Clay

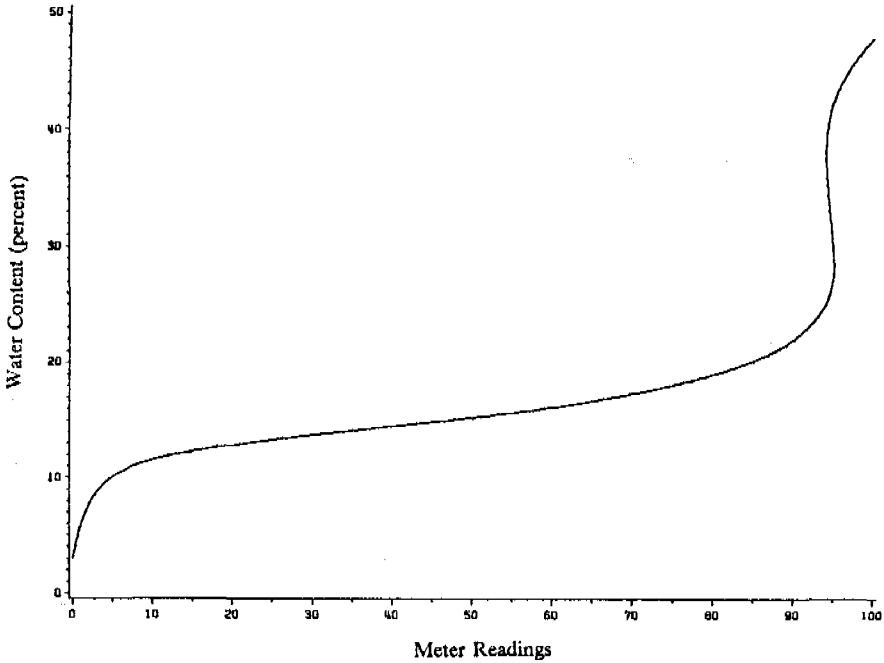

FIGURE 21
Grain Size Distribution Curve of Clay

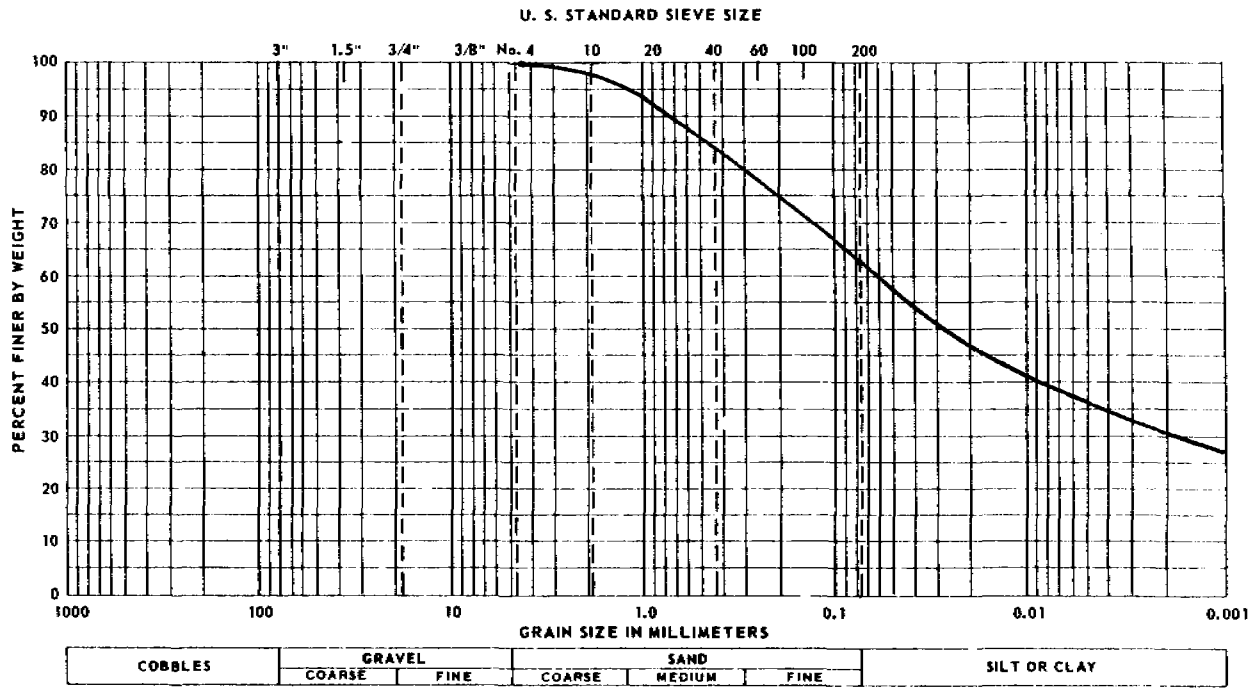

FIGURE 22
Placement of Soil Moisture Blocks in Clay

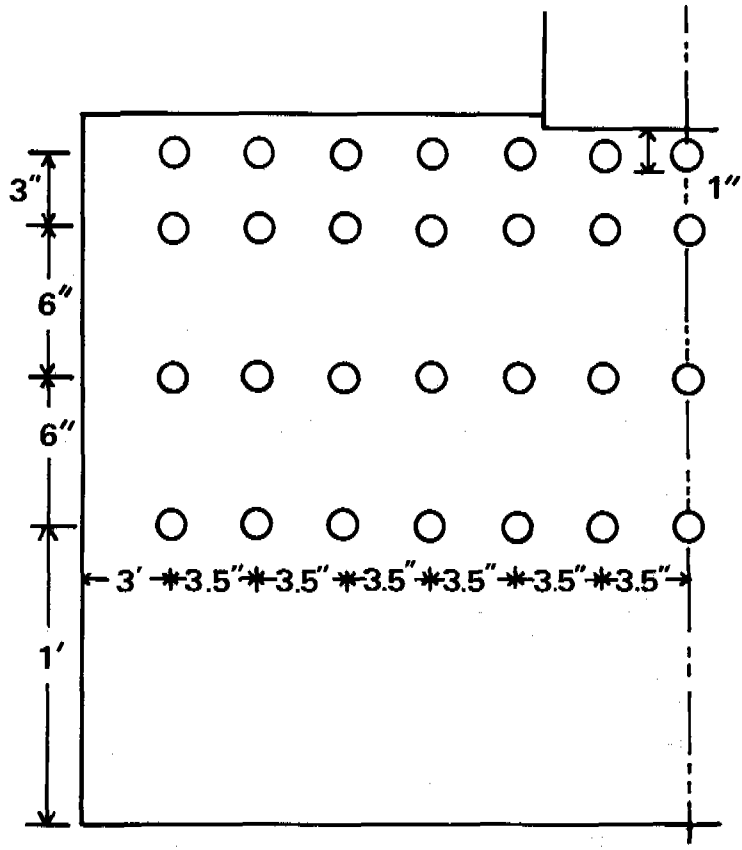

FIGURE 23
Results of First Clay Experiment (37 and 57 Minutes)

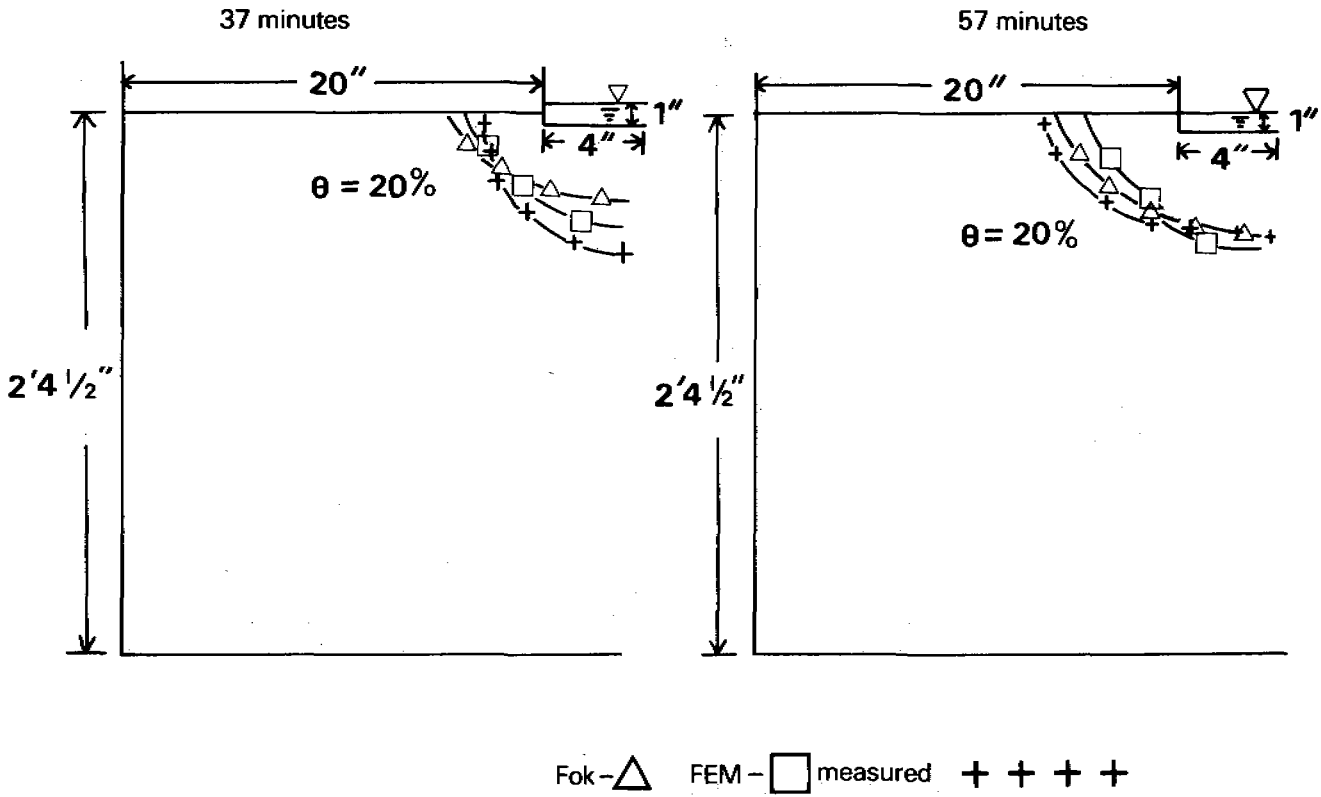

FIGURE 24
Results of First Clay Experiment (147 and 237 Minutes)

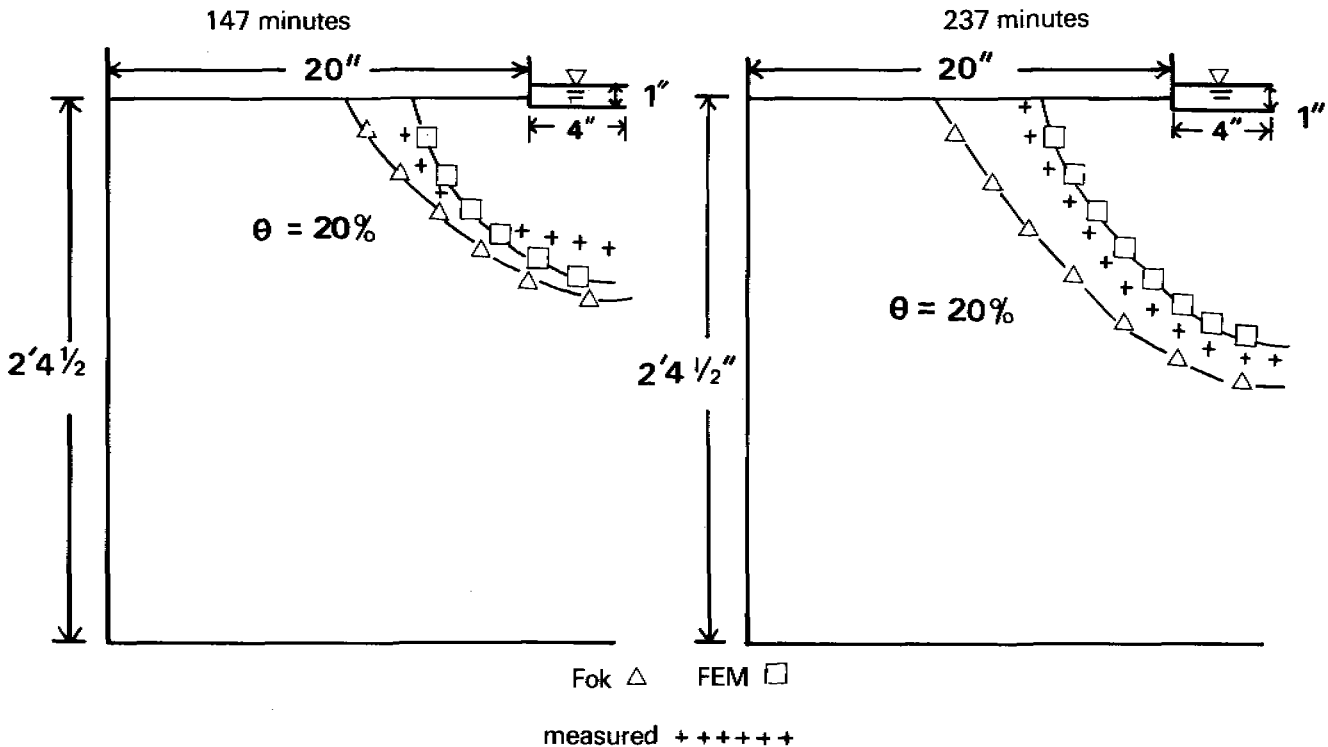

FIGURE 25
Results of Second Clay Experiment (39 and 84 Minutes)

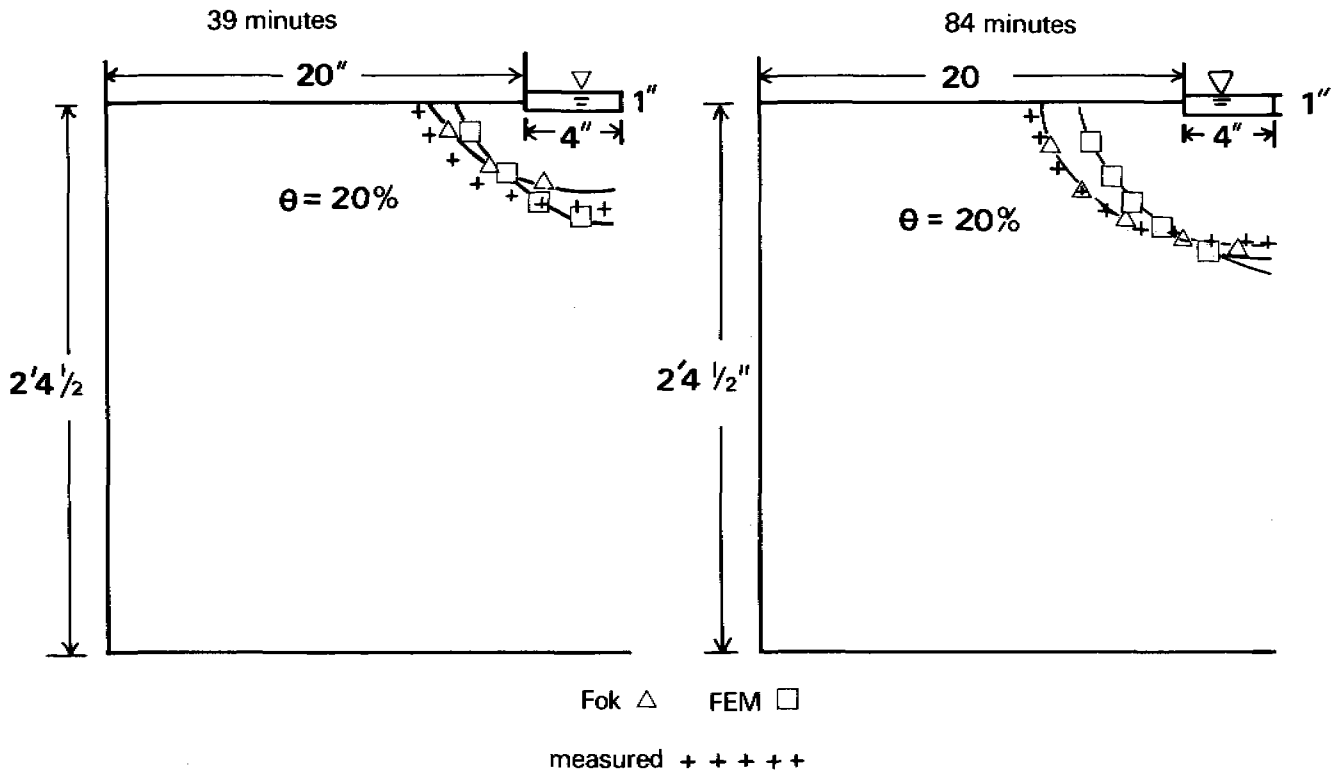

FIGURE 26
Results of Second Clay Experiment (164 and 224 Minutes)

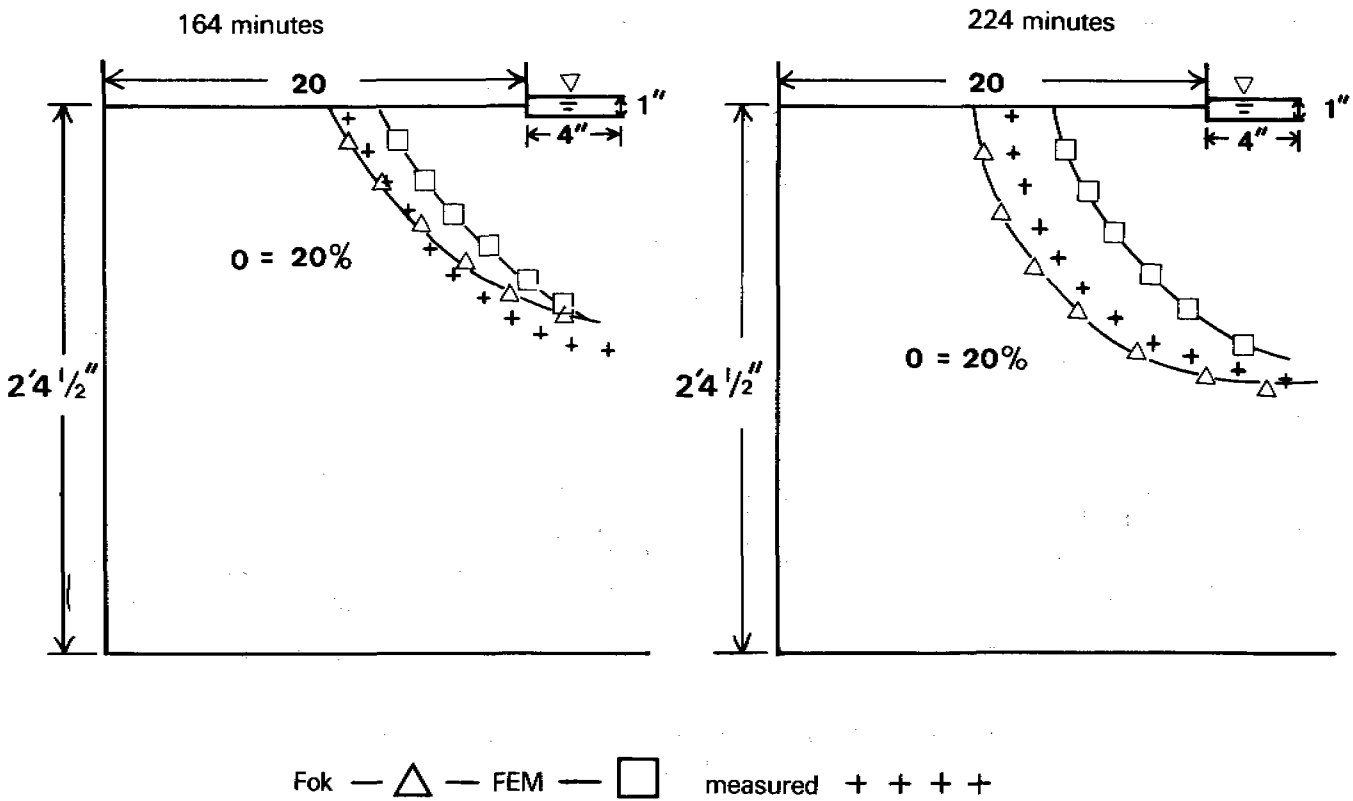

FIGURE 27
Water Content versus Meter Readings for Loam

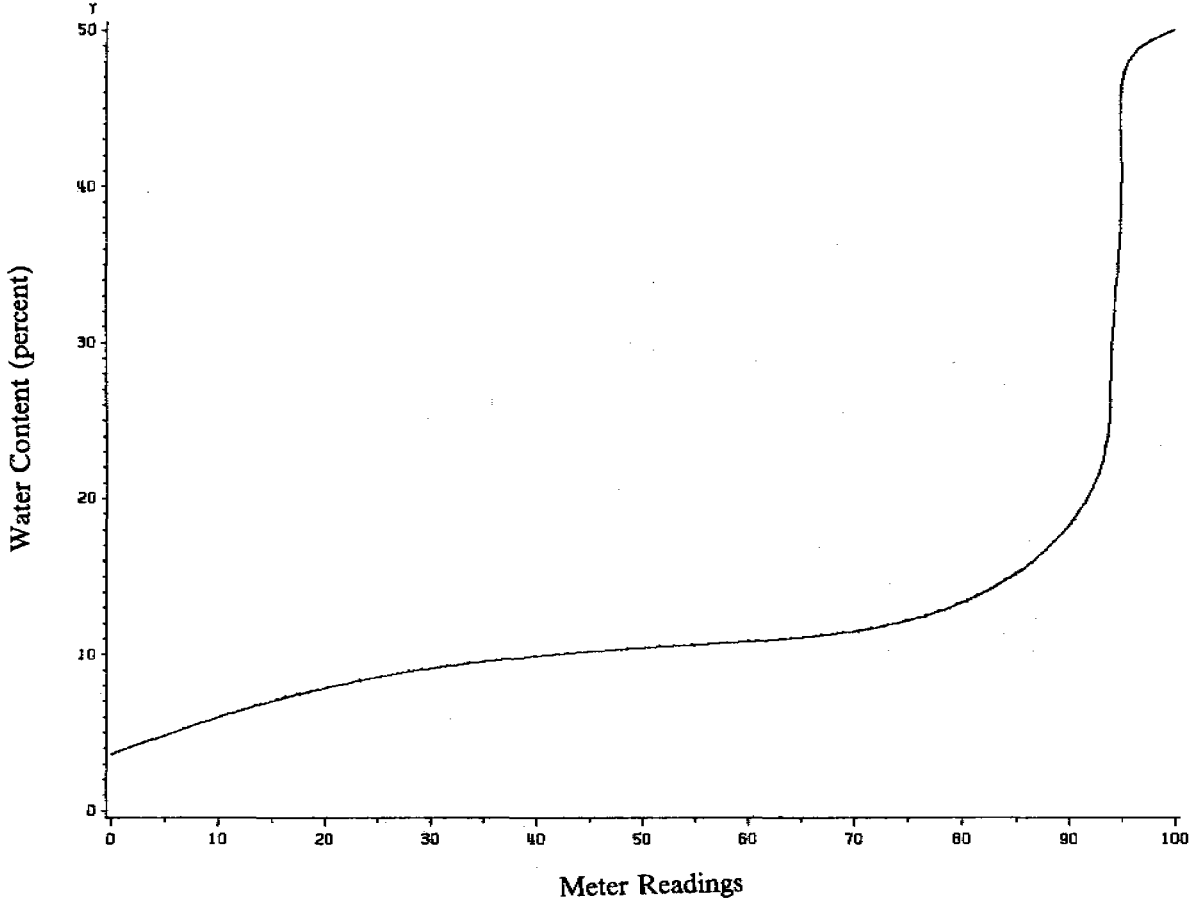

FIGURE 28
Grain Size Distribution Curve of Loam

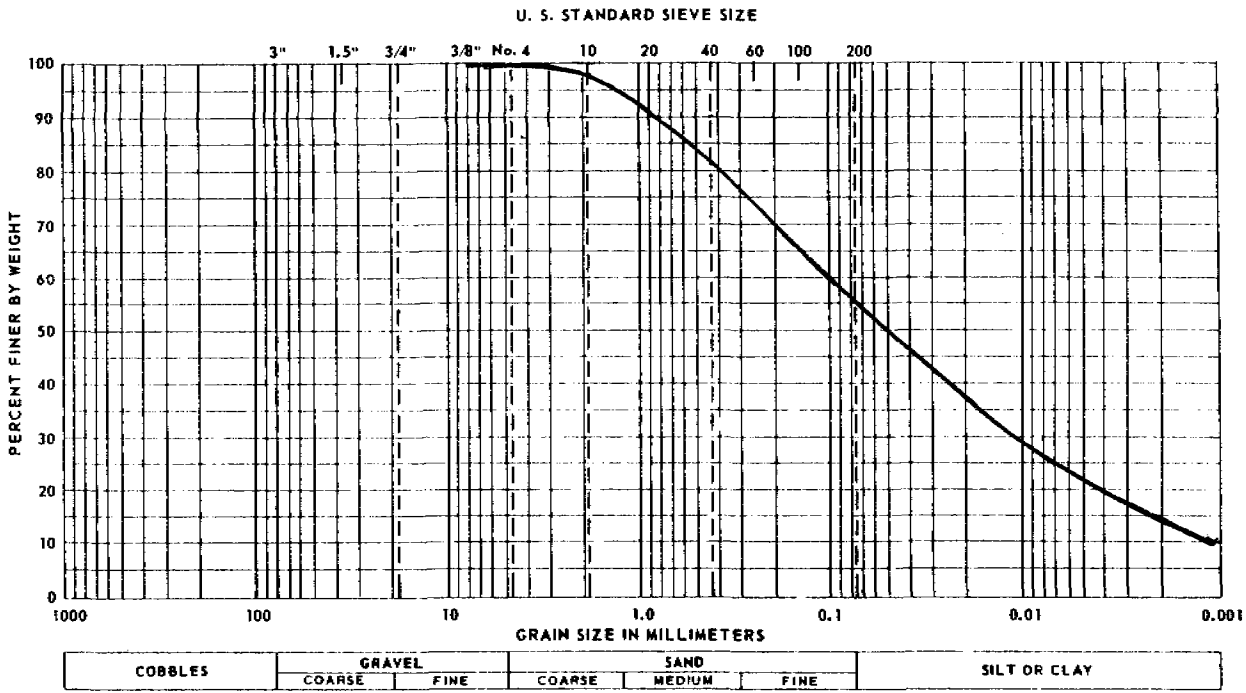

FIGURE 29
Placement of Soil Moisture Blocks in Loam

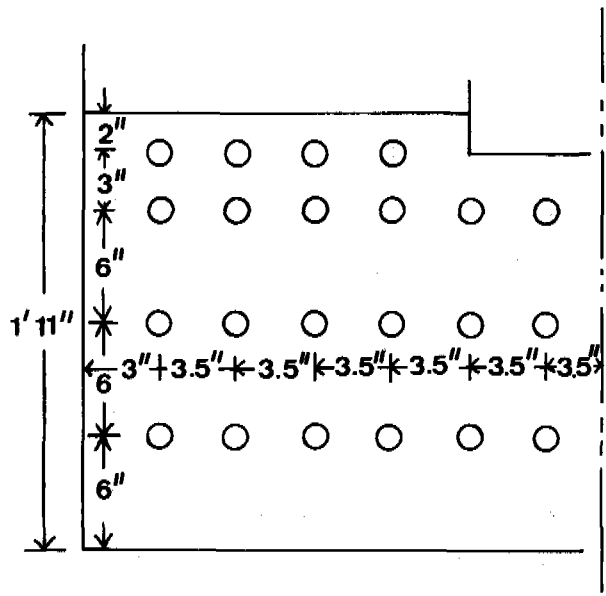

FIGURE 30
Results of Loam Experiment (2 and 10 Minutes)

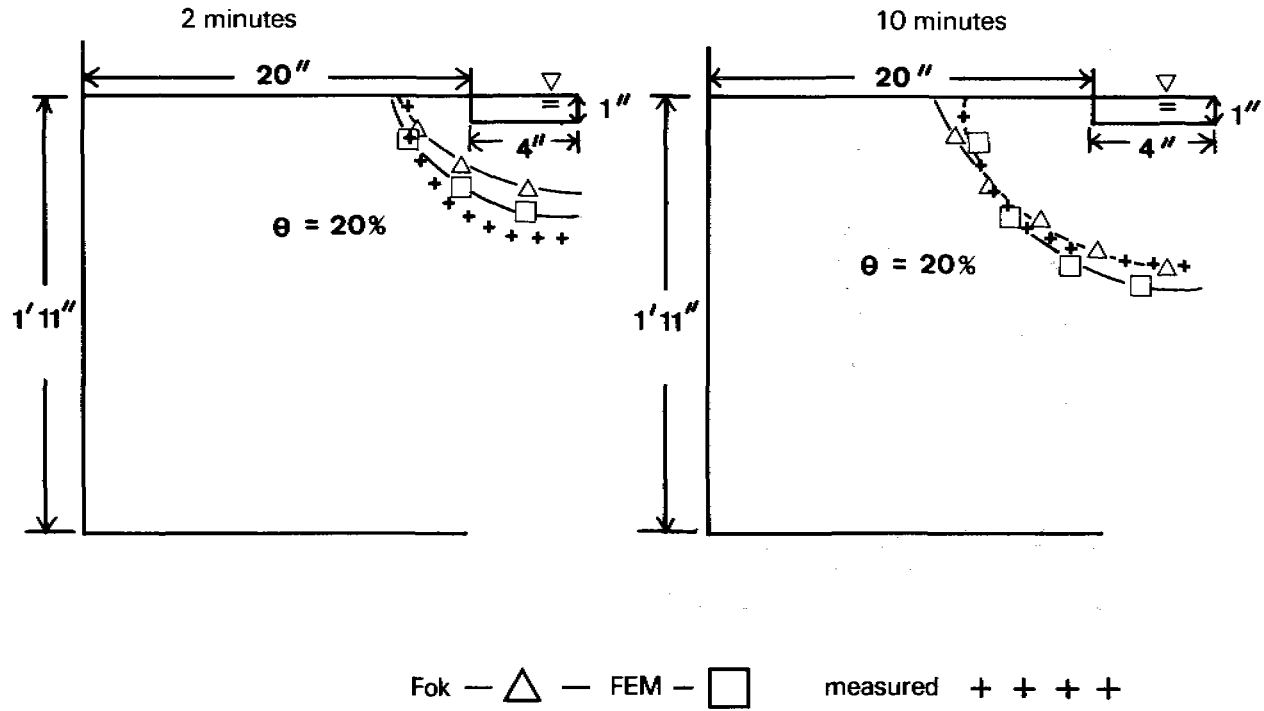

FIGURE 31
Results of Loam Experiment (25 and 60 Minutes)

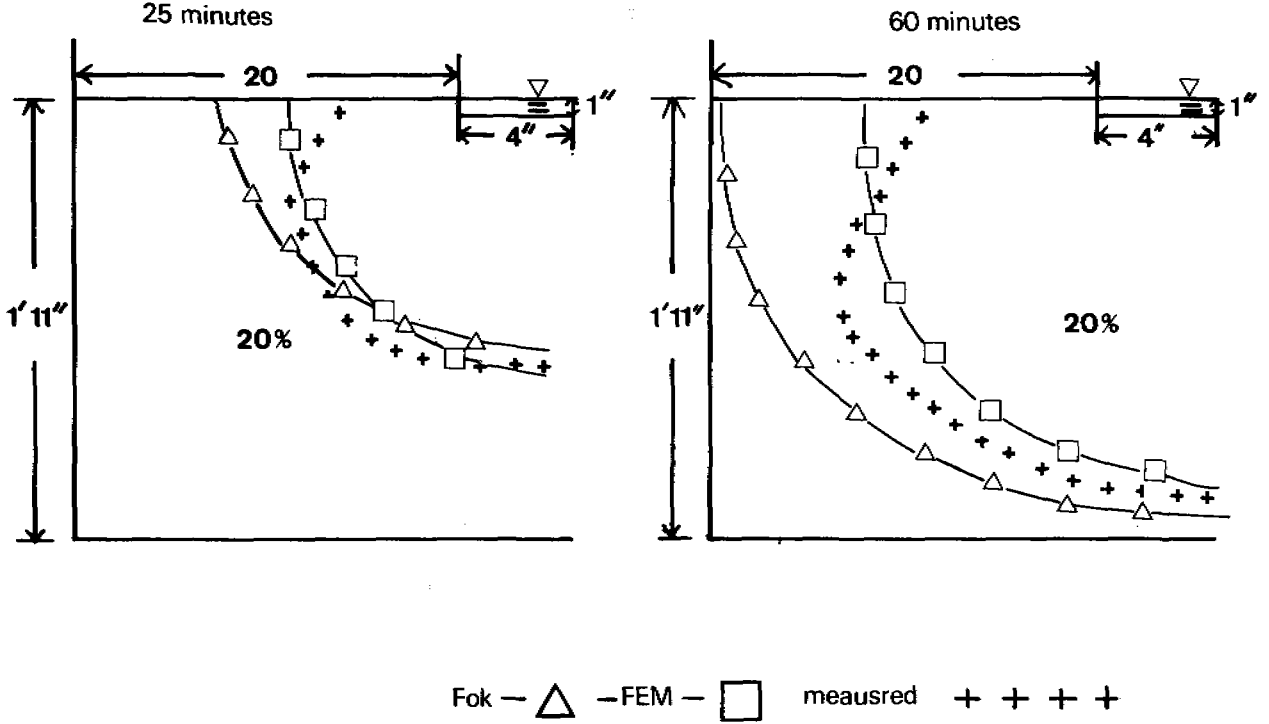

FIGURE 32
Geometry of the Trench for Parametric Studies

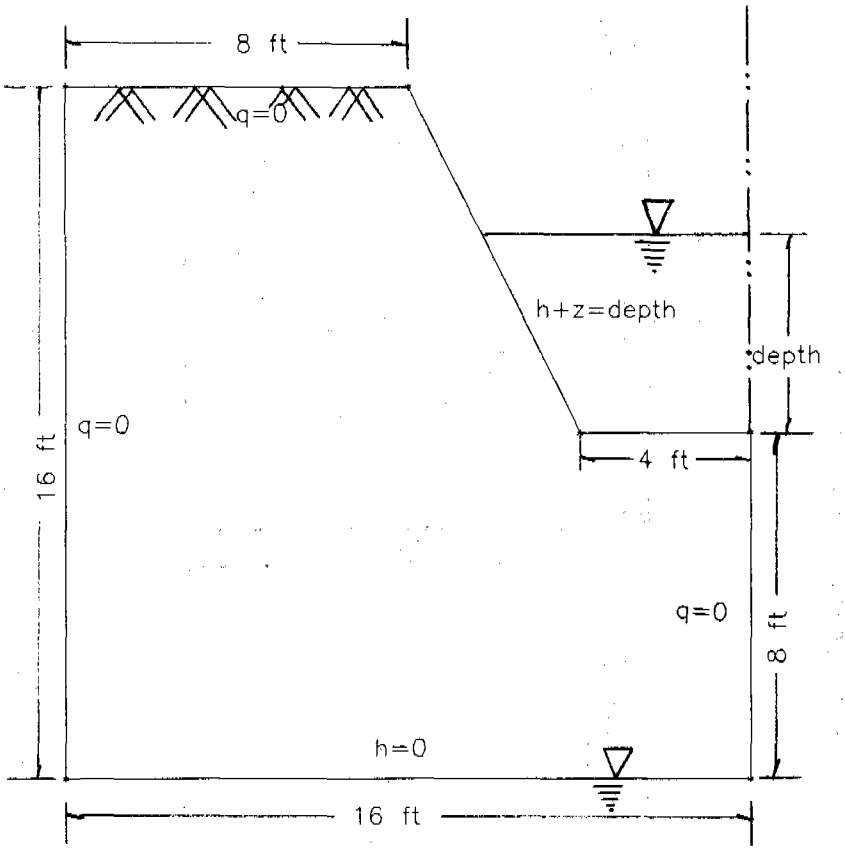

FIGURE 33
Inflow Hydrograph to the Trench Prescribed for Parametric Studies

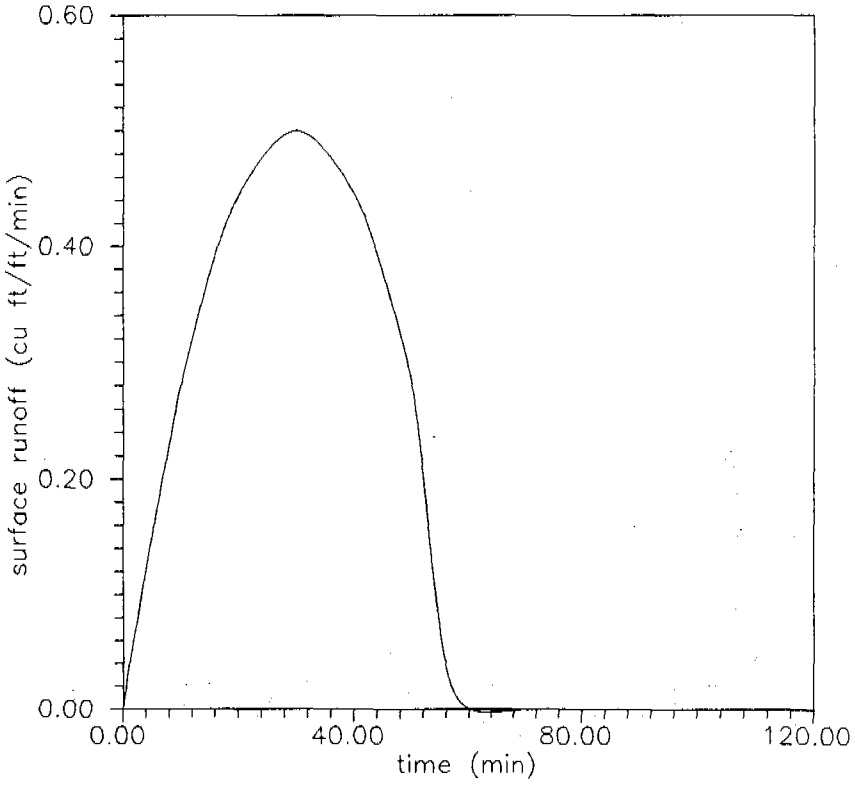

FIGURE 34
Infiltration Rates for Different Soils

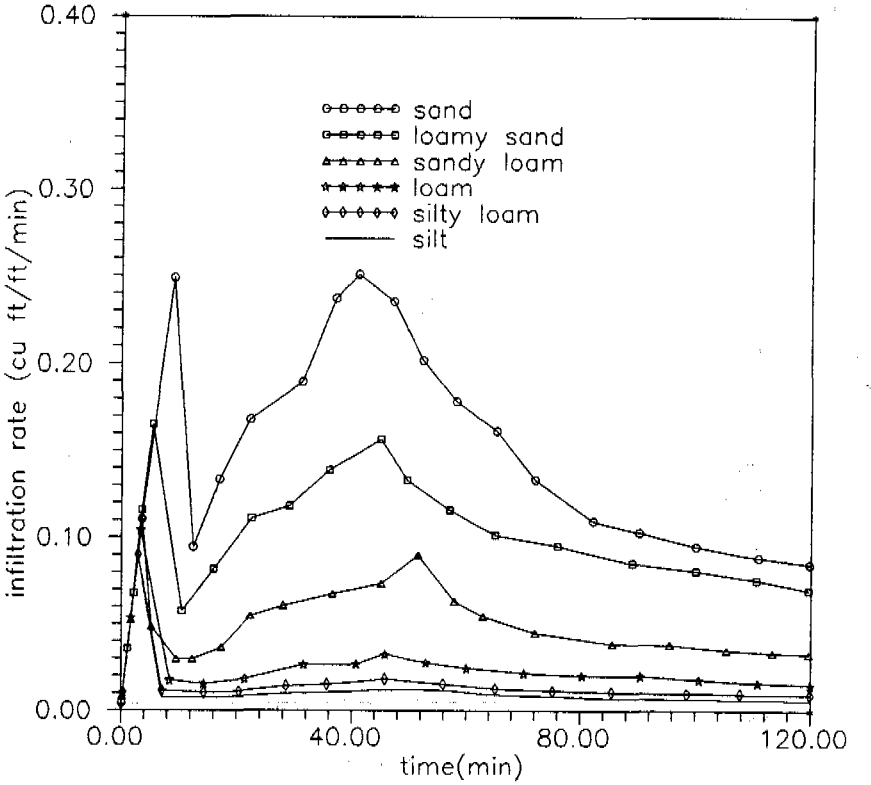

FIGURE 35
Water Levels in the Trench for Different Soils

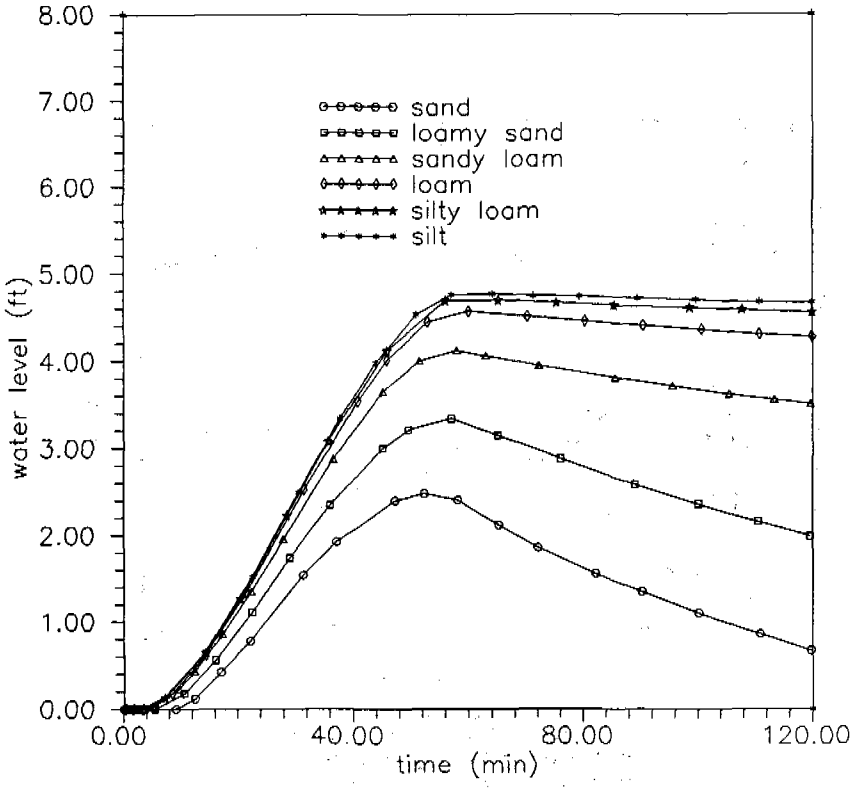

FIGURE 36

Effects of Deep/narrow vs. Shallow/wide Trench on Infiltration Rates and Water Levels in Trenches with Constant Volume (Sandy Loam Soil)

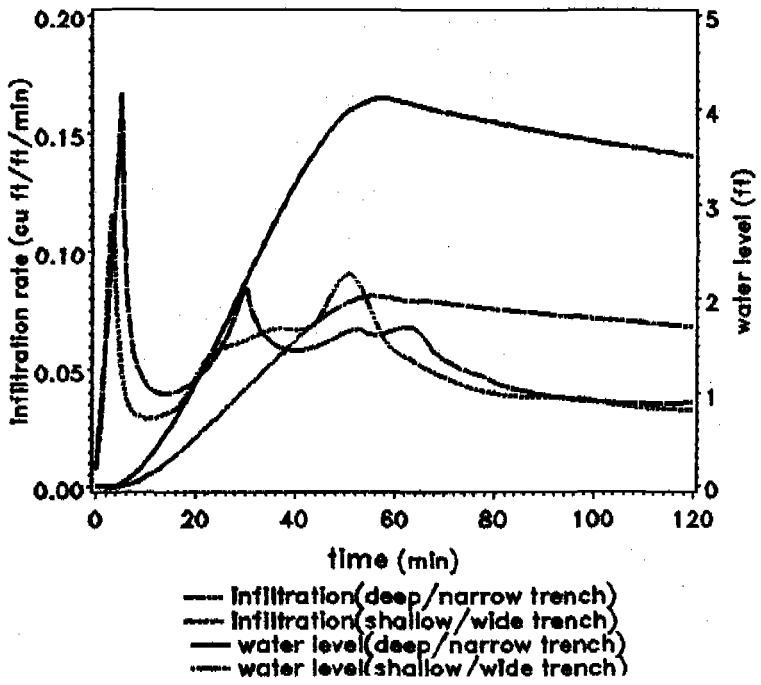

FIGURE 37

Effects of Deep/narrow vs. Shallow/wide Trench on Infiltration Rates and Water Levels in Trenches with Constant Volume (Loam Soil)

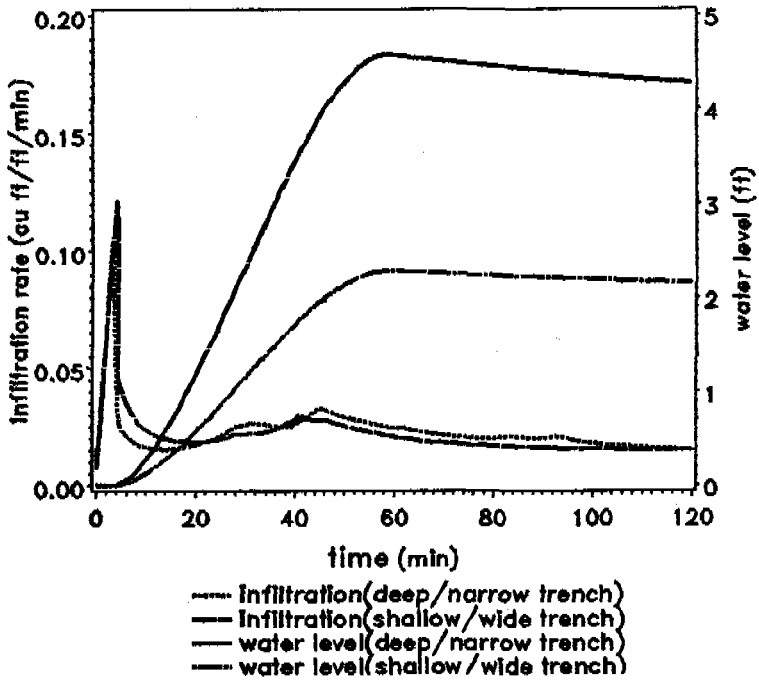

FIGURE 38
Effects of Long/narrow vs. Short/wide Trench on Infiltration Rates and Water Levels in Trenches with Constant Volume (Sandy Loam Soil)

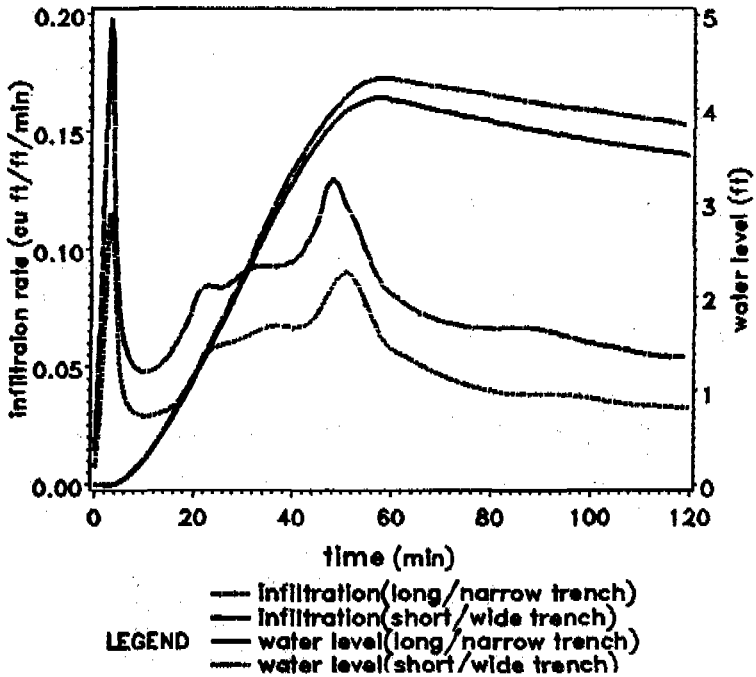

FIGURE 39

Effects of Long/narrow vs. Short/wide Trench on Infiltration Rates and Water Levels in Trenches with Constant Volume (Loam Soil)

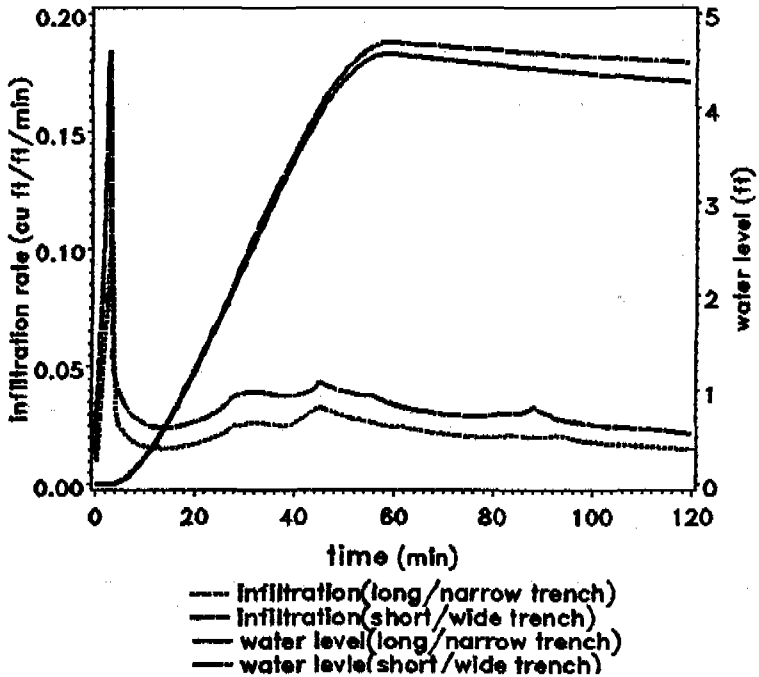

FIGURE 40
Effects of Water Table on Infiltration Rate

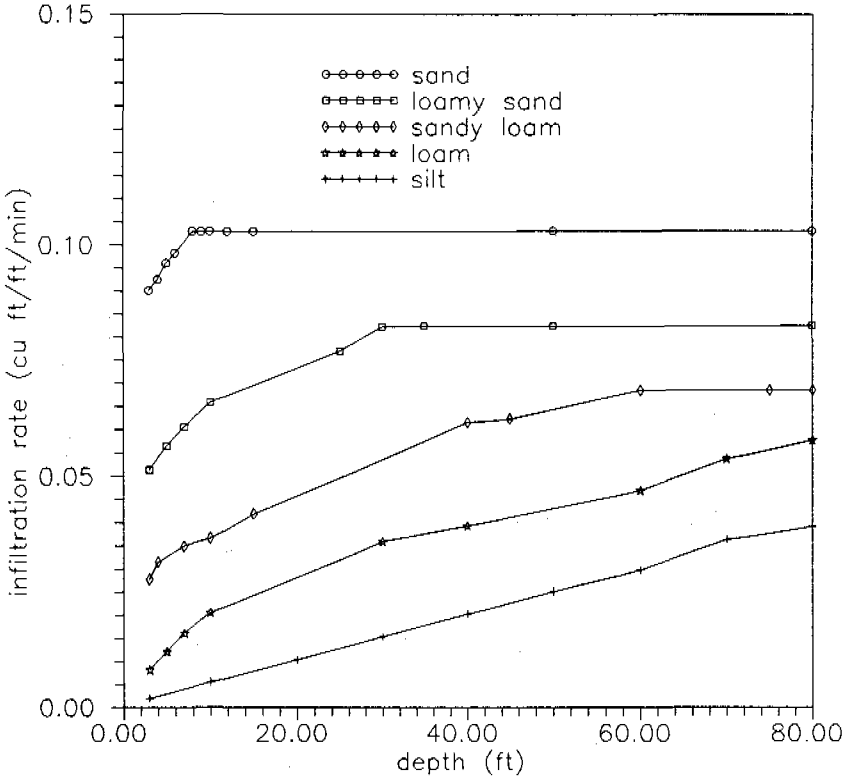

FIGURE 41
Effects of Sediment Deposition in Trench on Infiltration Rate

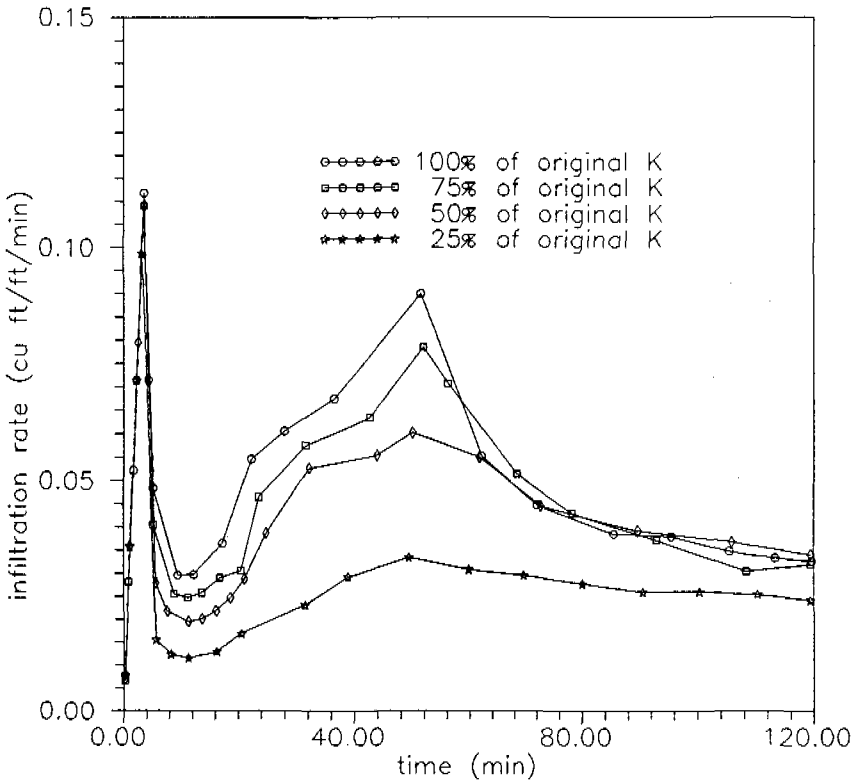

FIGURE 42
Long-term Simulation of Infiltration in a Trench

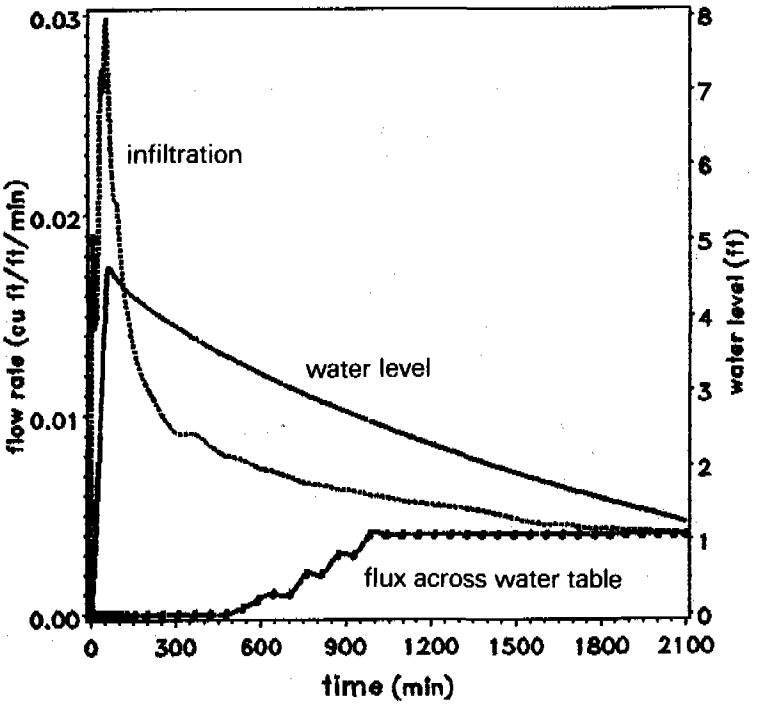

FIGURE 43
Movement of Wetting Fronts in Soil Medium as a Function of Time

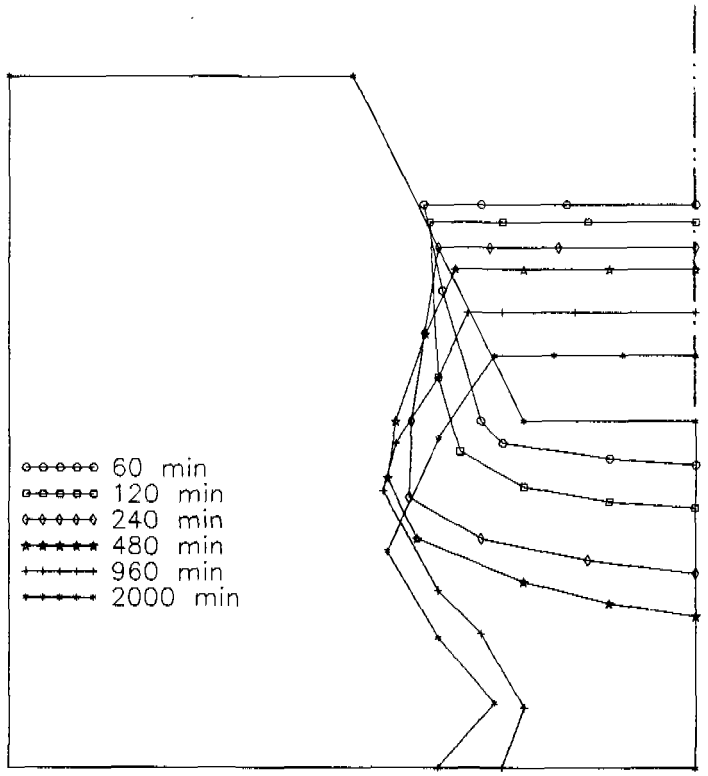

TABLES

TABLE 1
Typical Values of van Genuchten's Model

Soil	K_s(cm/h)	θ_s	θ_r	λ(cm^{-1})	ν
Clay	0.20	0.38	0.07	0.008	1.09
Clay Loam	0.26	0.41	0.09	0.019	1.31
Loam	1.04	0.43	0.08	0.036	1.56
Loamy Sand	14.60	0.41	0.06	0.124	2.28
Silt	0.25	0.43	0.03	0.016	1.37
Silty Loam	0.45	0.45	0.07	0.020	1.41
Silty Clay	0.02	0.36	0.07	0.005	1.09
Silty Clay Loam	0.07	0.43	0.09	0.010	1.23
Sand	29.70	0.43	0.04	0.145	2.68
Sandy Clay	0.12	0.38	0.10	0.027	1.23
Sandy Clay Loam	1.31	0.39	0.10	0.059	1.48
Sandy Loam	4.42	0.41	0.06	0.075	1.89

REFERENCES

American Society of Agricultural Engineers. 1983. *Advances in Infiltration.* Conference proceedings, Chicago.

Beukeboom, T.J. 1982. "A Dry-Well System for Excess Rainwater Discharge." *Proceedings of the International Symposium on Urban Hydrology, Hydraulics and Sediment Control.* Lexington, Kentucky.

Bouwer, H. 1978. *Groundwater Hydrology.* McGraw-Hill, Inc., New York.

Carsel, R.F., R.S. Parrish. 1988. "Developing Joint Probability Distribution of Soil of Water Retention Characteristics." *Water Resources Research.* 24:5, 755-769.

Eagleson, P.S. 1970. *Dynamic Hydrology.* McGraw-Hill, Inc., New York

Ericsson, L.O., and G. Gustafson. 1982. "Design of Stormwater Recharge Basins." *Proceedings of the Conference on Stormwater Detention Facilities.* Henniker, New Hampshire.

Fok, Y., and V.E. Hansen. 1966. "One-Dimensional Infiltration into Homogeneous Soil." *Journal of Irrigation and Drainage.* ASCE, 92:3, 35-48.

Fok, Y. 1967. "Infiltration Equation in Exponential Forms." *Journal of Irrigation and Drainage.* ASCE, 93:4, 125-135.

Fok, Y., S. Chung, and C.K. Clark. 1982. "Two-Dimensional Exponential Infiltration Equations." *Journal of Irrigation and Drainage.* ASCE, 108:4, 231-241.

Green, W.H., and G.A. Ampt. 1911. "Studies on Soil Physics.Part 1 — The Flow of Air and Water through Soils." *Journal of Agricultural Science.* Vol. 4, 1-24.

Hansen, V.E. 1955. "Infiltration and Soil Water Movement During Irrigation." *Soil Science,* 79:2, 93-105.

Hantzche, N.N., and J.B. Franzini. 1980 "Utilization of Infiltration Basins for Urban Stormwater Management." *Proceedings of the International Symposium on Urban Runoff.* Lexington, Kentucky.

Higgs, G.E. 1978. "A Case Study of Percolation Storage." *Proceedings of the International Symposium on Urban Stormwater Management.* Lexington, Kentucky.

Huyakorn, P.S., E.P. Springer, V. Guvanasen, and T.D. Wadsworth. 1986. "A Three-Dimensional Finite-Element Model for Simulating Water Flow in Variably Saturated Porous Media," *Water Resources Research,* 22:13, 1790-1808.

Kaluarachchi, J.J., and J.C. Parker. 1987, "Finite Element Analysis of Water Flow in Variably Saturated Soil." *Journal of Hydrology, 90: 269-291.*

Kim, J. 1986. A Study of Infiltration Trenches in Unsaturated Soil. Masters thesis, Virginia Polytechnic Institute and State University, Blacksburg.

Li, W. 1983. *Fluid Mechanics in Water Resources Engineering.* Allyn and Bacon, Inc.

Maryland Department of Natural Resources. 1984. *Standards and Specifications for Infiltration Practices.* Stormwater Management Division, Water Resources Administration.

McBride, M.C., and Y.M. Sternberg. 1983. *Storm Water Management Infiltration Structures.* Maryland Department of Transportation, State Highway Administration Research Report, No. AWO83-253-046.

Northern Virginia Planning District Commission. 1978. *Guidebook for Screening Urban Nonpoint Pollution Management Strategies.*

Northern Virginia Planning District Commission. 1987. *BMP Handbook for the Occoquan Watershed.*

Panikar, J.T., and G. Nanjappa. 1977. "Suction Head at Wet Front in Unsaturated-flow Problems — A New Definition." *Journal of Hydrology.* Vol. 33, 1-14.

Poertner, H.G. 1974. *Practices in Detention of Urban Stormwater Runoff.* American Public Works Association, Special Report No. 43.

Reddy, J.N. 1984. *An Introduction to the Finite Element Method.* McGraw-Hill, Inc. New York.

Schueler, T.R. 1987. *Controlling Urban Runoff: A Practical Manual for Planning and Designing Urban BMPs.* Metropolitan Washington Council of Governments.

Selim, H.M., and D. Kirkham. 1974. "Unsteady State Two-Dimensional Water Content Distribution and Wetting Fronts in Soils." *Geoderma,* 11, 259-274.

SoilMoisture Equipment Corporation. 1985. *Operating Instructions for the Model 5201 Soilmoisture Blocks.*

SoilMoisture Equipment Corporation. 1986. *2800 KI Operating Instructions.*

South Florida Water Management District. 1983. *Permitting Information Manual.* Vol. IV, Management and Storage of Surface Waters.

Toscoz, S.D., D. Kirkham, and E.R. Baumann. 1965. "Two-Dimensional Infiltration and Wetting Fronts." *Journal of Irrigation and Drainage.* ASCE, 91:3, 4477, 65-79.

Virginia Water Control Board. 1978. *Best Management Practices Handbook.*

van Genuchten, M.T. 1980a. "A Closed-form Equation for Predicting the Hydraulic Conductivity of Unsaturated Soils." *Soil Science Society of America Journal.* 44, 892-99.

van Genuchten, M.T. 1980b. "A Comparison of Numerical Solutions of the One-Dimensional Unsaturated-saturated Flow and Mass Transport Equations." *Proceedings of the Third International Conference on Finite Elements in Water Resources.* University of Mississippi.

Yeh, G.T. 1987. *FEMWATER: A Finite Element Model of Water Flow through Saturated-Unsaturated Porous Media.* Environmental Science Division, Publ. 2943, Oak Ridge National Laboratory.

Yim, C.S., and Y.M. Sternberg. 1984. *Laboratory Tests of Stormwater Management Infiltration Structures.* Maryland Department of Transportation, State Highway Administration Research Report, No. AWO84-288-046.